ISTANBUL TECHNICAL UNIVERSITY★GRADUATE SCHOOL OF SCIENCE ENGINEERING AND TECHNOLOGY

NUMERICAL ANALYSIS OF ADDITIVE MANUFACTURING OF MARAGING STEEL

M.Sc THESIS

MOBIN MAJEED

Department of Mechanical Engineering

Materials and Manufacture Graduate Program

DECEMBER 2018

ISTANBUL TECHNICAL UNIVERSITY ★ GRADUATE SCHOOL OF SCIENCE ENGINEERING AND TECHNOLOGY

NUMERICAL ANALYSIS OF ADDITIVE MANUFACTURING OF MARAGING STEEL

M.Sc. THESIS

MOBIN MAJEED
(503151323)

Department of Mechanical Engineering

Materials and Manufacture Graduate Program

Thesis Advisor: Prof. Dr. Murat Vural

DECEMBER 2018

ISTANBUL TEKNİK ÜNİVERSİTESİ ★ FEN BİLİMLERİ ENSTİTÜSÜ

YÜKSEK DAYANIMLI ÇELİĞİN 3 BOYUTLU YAZICI İLE İMALATININ SAYISAL ANALİZİ

YÜKSEK LİSANS TEZİ

MOBIN MAJEED
(503151323)

Makina Mühendisliği Anabilim Dalı

Malzeme ve İmalat Lisansüstü Programı

Tez Danışmanı: Prof. Dr. Murat Vural

ARALIK 2018

Mobin Majeed, a M.Sc. student of İTU Graduate School of Science Engineering and Technology student ID 503151323, successfully defended the thesis/dissertation entitled “Numerical analysis of additive manufacturing of maraging steel”, which he prepared after fulfilling the requirements specified in the associated legislations,

Thesis Advisor :	**Prof. Dr. Murat Vural** İstanbul Technical University	.....
Jury Members :	**Prof. Dr. Şafak Yılmaz** İstanbul Technical University	.....
	Prof. Dr. Cüneyt Fetvacı İstanbul University	.....

Date of Submission : 16 November 2018
Date of Defense : 6 December 2018

FOREWORD

I thank everyone for their support and guidance especially my advisor Prof. Murat Vurat who has supported me in every aspect from direction to finance. It was my pleasure to work with him. I leearned a lot of new things in Turkey and credit goes to whole manufacturing department including Prof. Safak Yilmaz and Prof. Turgut Gulmez. At last but not the least a special thanks to Hamaid M. Khan a PhD student from Istanbul University who supported me to learn the ANSYS software, that was very useful in my thesis.

December 2018

Mobin Majeed
(Mechanical Engineer)

TABLE OF CONTENTS

Page

FOREWORD ..... **vii**
TABLE OF CONTENTS ..... **ix**
ABBREVIATIONS ..... **xi**
SYMBOLS ..... **xiii**
LIST OF TABLES. ..... **xv**
LISTOF FIGURES. ..... **xvii**
SUMMARY. ..... Error! Bookmark not defined.**x**
ÖZET ..... Error! Bookmark not defined.**iii**
1. INTRODUCTION. **1**
1.1 The Advantages of Additive Manufacturing 2
1.2 The Disadvantages of Additive Manufacturing 4
1.3 Market Perspective and Application 4
1.3.1 New initiatives in the market 6
1.4 Applications of Additive Manufacturing 8
1.4.1 Medical application 8
1.4.2 Aerospace and defense sector 9
1.4.3 Automotive 9
2. LITERATURE REVIEW **11**
2.1 Interaction of Heat Source with Powder 11
2.2 Mechanism of Heat and Mass Transfer 13
2.3 Boundary Conditions 14
2.4 Role of Non-Dimensional Numbers 14
3. CLASSIFICATION OF ADDITIVE MANUFACTURING **16**
3.1 Based on Heat Source Used for Additive Manufacturing 16
3.1.1 Laser beam melting (selective laser melting) 17
3.1.2 Electron beam melting (EBM) 19
3.1.3 3 D printing 20
3.1.4 Direct energy deposition (laser metal deposition) 21
4. MATERIALS FOR ADDITIVE MANUFACTURING **22**
4.1 Non Standard Materials 22
4.2 Stainless Steel 23
4.3 Construction and Tools Steel 23
4.4 Super Alloys 23
4.5 Light Alloys 24
4.5.1 Almunium (AlSi10Mg) 24
4.6 Maraging Steel 25
5. STEPS IN ADDITIVE MANUFACTURING **29**
5.1 CAD Model Generation Based on Design 29
5.2 Conversion of CAD File to an Acceptable AM File Format 30
5.3 CAD Model Preparation 30
6. MICROSTRUCTURE AND MELT POOL **33**
6.1 Maraging Steel Microstructure 33

6.1.1 Hardening of maraging steel 35
6.2 Crystallographic Texture of AlSi10Mg 36
7. EFFECTS OF PARAMETERS ON ADDITIVE MANUFACTURING 39
7.1 Surface Roughness and Density Optimization 39
7.2 Effect of Scanning Strategy on Microstructure 39
7.3 Effect of Oxygen 41
7.4 Effect of Power and Scan Speed 42
7.5 Effect of Relative Density 43
7.6 Effect on Surface Quality 43
7.7 Effect on Hardness 44
8. DEFECTS IN ADDITIVE MANUFACTURED PARTS 45
8.1 Fracture 45
8.2 Porosity and Lack of Fusion 45
8.3 Surface Roughness 47
8.4 Delamination and Cracking 48
9. MELT POOL MODELING OF MARAGING STEEL 49
9.1 Modeling and Meshing of Structure 50
9.2 Paremeters in Analysis 52
9.3 Results of Analysis in ANSYS 53
10. CONCLUSION 63
REFERENCE 65
CURRICULUM VITAE 69

ABBREVIATIONS

AM **:** Additive Manufacturing

CAD **:** Computer Aided Design

CNC **:** Computer Numeric Control

EBM : Electron Beam Melting

LBM **:** Laser Beam Melting

LMD **:** Laser Metal Deposition

SEM **:** Scanning Electron Microscopy

SSS **:** Solid State Sintering

SLM : Selective Laser Melting

VD **:** Volume Diffusion

SYMBOLS

f	: Distribution Factor
r_b	: Heat Source Radius
η_p	: Fraction of energy absorbed by powder
η_1	: Absorption Coefficient of Deposit
t_1	: Layer Thickness of Powder
u_i, u_j	: Velocity Components
ρ	: Density
t	: Time
x_i	: Distance Along i Direction
S_j	: Source term of momentum equation
μ	: Dynamic Viscosity
C_p	: Specific Heat
h	: Sensible Heat
ΔH	: Latent Heat
k	: Thermal Conductivity
Υ	: Surface Tension
T_m	: Marangoni Stress
u_i	: Velocity Component in I Direction
r	: Radial distance from axis of heat source

LIST OF TABLES

Page

Table 4.1 : Composition of AlSi10Mg. ……..…….……..…….…..**25**
Table 4.2 : Composition of Maraging steel 300. …….…….**.....27**
Table 4.3 : Commonly used alloys in AM and their chemical composition. ….**.....27**
Table 9.1 : Properties of maraging steel solid and powder. …..…….**.....54**
Table 9.2 : Result of temperature and melt pool at different combination of power and speed. ……..…….....…**57**

LIST OF FIGURES

Page

Figure 1.1 : Gas turbine manufactured by selective laser melting..... **1**
Figure 1.2 : Synonyms and classification of additive manufacturing. **2**
Figure 1.3 : (a) Hydraulic prototype, (b) LBM fabricated prototype, (c) Support of satellite (d) Ti6Al4V implant with particular surface design.....…..….**3**
Figure 1.4 : Region wise revenue generation from 2015 to 2025. ..... **6**
Figure 1.5 : Percentage of market share of various countries around the world in 2015. ..... **7**
Figure 1.6 : A human skin generated from 3 D printing using stem cells. **8**
Figure 1.7 : Damaged part of skeletal replaced by AM part..... **9**
Figure 1.8 : A model of jet engine built by AM. **10**
Figure 1.9 : BMW car and hand tool manufactured by AM. **10**
Figure 2.1 : Density distribution with varying value of f. **11**
Figure 2.2 : Interaction of laser with powder (a) after ejection for DED (b) In powder bed. **12**
Figure 2.3 : Mechanism of heat transfer. **13**
Figure 3.1 : Process of additive manufacturing. **17**
Figure 3.2 : SLM machine with flow directions (by SLM solutions). **18**
Figure 3.3 : Interior view of SLM machine components. **19**
Figure 3.4 : Mechanism of powder diffusion in SSS. **19**
Figure 3.5 : Schematic diagram of electron beam melting main components. **21**
Figure 3.6 : Direct metal deposition process. **22**
Figure 4.1 : Materials for AM developed by EOS and their area of application. **23**
Figure 4.2 : SEM image of powder particles for morphology comparison. **26**
Figure 4.3 : SEM image of maraging steel 300 powder. **27**
Figure 5.1 : Steps involved in rapid prototyping. **29**
Figure 5.2 : An example of part in STL format. **30**
Figure 6.1 : Track remelting and layer overlapping in SLM. **33**
Figure 6.2 : Direction representation of scan track. **34**
Figure 6.3 : Micrograph of etched maraging steel (a) top/cs2 side (b) cs1 side. **34**
Figure 6.4 : SEM image of maraging steel (a) cs2 side (b) cs1 side. **35**
Figure 6.5 : Martensite structure after heat treatment. **36**
Figure 6.6 : ESDB graph of AlSi10Mg part with front view(left) and top view(Right). **36**
Figure 6.7 : Front and side view of microstructure of AlSi10 Mg. **37**
Figure 7.1 : Scanning strategies for selective laser melting. **40**
Figure 7.2 : Top view of sample B with bidirectional strategy. **40**
Figure 7.3 : Oxygen trapped in SLM part. **41**
Figure 7.4 : Laser speed vs power optimization. **42**
Figure 7.5 : Effect of scan speed on density. **43**
Figure 7.6 : Effect of scan speed on surface roughness. **43**
Figure 7.7 : Rockwell and vickers hardness test of specimens. **44**
Figure 8.1 : Broken tensile surface (a) as built sample (b) sample aged at 460^{o} C . **45**
Figure 8.2 : (a) Keyhole porosity (b) lack of fusion and gas entrapment porosity. . **46**
Figure 8.3 : (a) Effect of speed on porosity (b) effect of power on porosity. **46**
Figure 8.4 : Balling phenomena. **47**

Figure 8.5 : Cracking (a & b) and delamination (c) in additive manufacturing. **48**
Figure 9.1 : ANSYS APDL software user interface **49**
Figure 9.2 : Element built structure of PLANE55 and SOLID70. ..... **50**
Figure 9.3 : ANSYS modeling and meshing. **51**
Figure 9.4 : Solid base and powder above solid geometry. **52**
Figure 9.5 : Parameters used in the analysis. **53**
Figure 9.6 : Melt pool at 1st incident laser. **54**
Figure 9.7 : Melt pool shape at the end of scanning of first layer. **55**
Figure 9.8 : Melt pool shape at the end of scanning of second layer. **55**
Figure 9.9 : Melt pool shape at the end of scanning of third layer. **56**
Figure 9.10 : Temperature variation of layers with 80 W power and different speed. **57**
Figure 9.11 : Temperature variation of layers with 100 W power and different speed. **58**
Figure 9.12 : Temperature variation of layers with 120 W power and different speed. **58**
Figure 9.13 : Temperature variation of layers with 80 W power and different speed. **59**
Figure 9.14 : Temperature variation of layers with 100 W power and different speed. **60**
Figure 9.15 : Temperature variation of layers with 120 W power and different speed. **60**

NUMERICAL ANALYSIS OF ADDITIVE MANUFACTURING OF MARAGING STEEL

SUMMARY

The usage of Additive Manufacturing (AM) is very recently expanded with most of the major companies located in the vicinity of Europe and nearby. It is now possible to manufacture complex metallic geometries and the process is not only restricted to prototypes. Additive manufacturing is now making a revolution in most of the manufacturing companies for example automotive, aerospace industry, energy sector, medical instruments and tooling. It has advantage as any product can be built in minimum assemblies some time in 1 pass not requiring any assembly at all.

In additive manufacturing a layer of fine powder is being melted and consolidated with the use of laser or electron beam. Then another powder layer is arranged and selectively melted on the previous layer. The process is repeated again and again in order to achieve the required height of built part. AM can be many types including EBM, LBM, DED and 3 D printing depending on the power source used and process of application of powder.

The procedure of AM starts from a simple 3 D CAD file. The file is then converted to the another format compatible for additive manufacturing machine. This format is STL file. STL file converts the CAD model into small triangles of different sizes and stores their location as well as interior and exterior of parts. Based on the information stored in STL file, the model is divided into small slices of equal height. The part geometry is constant with one slice. The sliced data is then transfer to additive manufacturing system for part fabrication.

In selective laser melting process power from laser selectively melts the metal and that forms a liquid melt pool. The melt pool suddenly solidifies as the laser passes that area. The successive melting of powder by consecutive tracks forms 1 layer. These layers are together consolidated one above other to form the solid geometry according to the data of CAD model (Figure 6.1). For strong bond of tracks and adjacent layer partial remelting of previous layer and overlapping of scan track is done. This also leads to higher densification and uniform properties with required degrees of isotropy.

Some of the mostly used materials in this filed are AlSi10Mg, Ti6Al4V, stainless steel and maraging steel. Most common material among these is AlSi10Mg. The reason behind this popularity is its low weight combined with high strength and fracture toughness. Its main application is in automotive and aerospace engineering. A lot of research has been done related to AlSi10Mg, Ti6Al4V etc. While the area of maraging is still remain unexplored. This is the reason that maraging steel has been chosen for analysis in AM. The purpose of this thesis is to analyze the melt pool shape and size considering some common parameters of power, speed, spot size, penetration depth etc.

In SLM cooling rate is fast so sudden solidification restricts formation of lath martensite in maraging steel. Large inclusions of titanium and aluminum combined oxides (TiO_2:Al_2O_3) are present with size 10 to 20 µm. These are responsible for

lowering the mechanical properties in aged conditions. As built maraging steel part is a ductile low carbon body centered cubic and has a martensitic structure. The relatively better strength and toughness of maraging steel is achieved by age hardening and aging. The aging process uniformly distribute the fine nickel rich intermetallic precipitates. These precipitates are the reason behind the strengthening of martensitic structure. And this precipitates also restricts the reversion of martensite to austenite and ferrite.

During solidification elongated grains grows towards the center of the melt pool (Figure 6.6). Epitaxial growth occurs only at some places like center of melt pool. Far from the center small nucleated grains forms. Few grains can grow towards the center of melt pool. Equiaxed grains forms at the top of melt pool. Next scanning layer remelts again the previously solidified layer which results in the disappearance of equiaxed grains from the top of melt pool. This causes only grains remain are those on the top layer of last melt pool.

There are various factors that affects the performance of additive manufacturing like the density increases with increasing scan speed and reaches a maximum value. The maximum point of density varies with different scan speeds. The density vs scan speed shows a parabolic pattern. For higher laser power, minimum lower surface roughness reaches at lower scan speed. If melt pool remains stable surface quality improves by increasing energy density.

Generally, laser is applied with different scanning strategies. Surface roughness, porosity level, microstructure and heat buildup depends mainly on scanning strategy. Different scanning strategies are unidirectional scanning, bidirectional scanning, rotation of scanning direction between 2 layers, dividing the scanning area into small islands called island scanning.

Oxygen reacts with molten metal at high temperature and forms metal oxide. The metal oxide is mainly found at the edges because of the continuous melting at top and bottom. Most of the metal oxides in additive manufacturing are found in aluminum as they are hard to break. In order to avoid the trapping of oxygen and oxide formation, it is recommended to use high incident heat which will melt the oxide film on the previous layer. Better scanning strategies and scanning parameter, use of noble gases like argon can significantly control the formation of oxide.

By increasing the energy per unit length P/v, melt pool volume become bigger and viscosity reduces. While decreasing P/v, recoil pressure become significant and distort scan tracks. By further increasing the scan speed energy given is not enough to fully melt powder and partially melt the substrate. Which results in instability and formation of droplets.

Relative density decreases with increasing scan speed. The reason of this decrease in density is the reduction of energy supplied per unit area by laser. Although this reduction is not significant at lower scan speed. Various analysis shows that by increasing the layer thickness from 30 μm to 40 μm results in 25 % reduction in scanning time while very little reduction in density. By much lowering scan speed, reduction in density is obtained due to balling effect.

The main purpose of this thesis is the modeling of melt pool, estimation of temperature profile, maximum temperature and melt pool depth in maraging steel additive manufacturing components. Study and simulation is done using APDL part of ANSYS

analysis software. Before starting the analysis material properties such as elastic modulus, young modulus, density, initial temperature, thermal conductivity, specific heat, coefficient of thermal expansion etc. are entered into the software either using user interface or ANSYS codes. On the basis of input data, the problem is being solved and further post processing is done in order to view the results, plot the necessary graphs.

In the present study two element types PLANE55 and SOLID70 are chosen. PLANE55 (Figure 9.2) is designed for steady state or transient thermal analysis and having single degree of freedom temperature at each node. Similarly, the same conditions apply to SOLID70 (Figure 9.2) except that it is used for 3D analysis. In present analysis a small cuboidal shape model is chosen to do the analysis. Model is having the dimensions of x = -0.6e-3 mm, y = 1.25e-3 mm, z = -0.8e-3 mm.

For performing an analysis in ANSYS it is necessary to divide the part into small meshes. The main purpose of meshing is to perform efficient, accurate and micro analysis. Whole load which is being applied on body is distributed in each mesh and analysis is done in every mesh. Convergence, accuracy and speed is dependent on meshing. In present analysis, multizone method is used. As it divides the geometry into small cubes. Finer mesh takes more time for analysis. To avoid time consumption, coarse mesh is used on part of body with little interest while finer mesh is done on the area of interest. The maximum number of nodes formed are 39401 and elements are 36818.

In this case the power input is taken as 80, 100, 120 W combined with scan speeds of 400, 600, 800, 1000 mm/s. The thickness of 1 layer is 30 µm. When laser is incident upon the powder layer it penetrates till certain depth into the powder as well as previously formed layer. The effect of this penetration leads to the re melting of previously formed layer of powder which results in melt pool depth of approximately 3 layers thick generally. So in this study penetration depth is assumed as 100 µm. The diameter of incident laser or spot diameter is taken as 100 µm.

The properties of maraging steel are fixed and don't change with temperature. While during analysis temperature dependent properties are taken into account. The melt pool shape, size and temperature distribution is shown in the following figure 9.10 to figure 9.15. Analysis is done using 3 layers of maraging steel as including more layers will increase the simulation time. .

The temperature and melt pool behavior is simulated for 3 layers and combination of power and speed. Table 9.12 shows the achieved temperature and melt pool depth result of simulation based on these combinations of power and speed. The results of temperature as well as melt pool depth versus layers is being plotted. Figure 9.10 to figure 9.12 shows the behavior of temperature. While figure 9.13 to figure 9.15 shows the behavior of melt pool depth. It has been found that temperature and melt pool depth increases with addition of further layers. Also both of these found to be decreasing by increasing the speed. This may be attributed to decrease in value of energy per unit volume available by increasing the speed while keeping other parameters constant.

YÜKSEK DAYANIMLI ÇELİĞİN 3 BOYUTLU YAZICI İLE İMALATININ SAYISAL ANALİZİ

ÖZET

Eklemeli İmalat (Eİ) kullanımı, yakın zamanda Avrupa ve yakın çevresinde bulunan büyük şirketlerin çoğu tarafından genişletilmiştir. Artık karmaşık metalik geometrilerin üretilmesi mümkün ve proses sadece prototiplerle sınırlı değildir. Eklemeli imalat günümüzde otomotiv, havacılık ve uzay endüstrisi, enerji sektörü, tıbbi cihazlar ve alet ile işleme gibi imalat şirketlerinin çoğunda çok yaygınlaşmıştır. Herhangi bir ürün herhangi bir montaj gerekmeden veya bazen 1 geçişte minimum montajla inşa edilebileceği için avantaj oluşturmaktadır.

Eklemeli imalatta, bir ince toz tabakası lazer veya elektron ışını kullanımıyla eritilir ve birleştirilir. Daha sonra başka bir toz tabakası oluşturulur ve önceki tabaka üzerinde titizlikle eritilir. İşlem, inşa edilen parçanın istenen yüksekliğini elde etmek için defalarca tekrarlanır. Eİ, kullanılan güç kaynağına ve toz uygulama işlemine bağlı olarak EBM, LBM, DED ve 3B baskı dahil birçok türde olabilir.

EÜ prosedürü basit bir 3 boyutlu CAD dosyasından başlar. Bu dosya daha sonra, eklemeli imalat makinesi için uyumlu bir başka formata dönüştürülür. Bu format STL dosyasıdır. STL dosyası, CAD modelini farklı boyutlarda küçük üçgenlere ayırır ve konumlarının yanı sıra parçaların iç ve dış kısımlarını da depolar. STL dosyasında saklanan bilgilere göre, model eşit yükseklikte küçük dilimlere bölünür. Parça geometrisi bir dilim ile sabittir. Dilimlenmiş veri, daha sonra parça üretimi için eklemeli imalat sistemine aktarılır.

Selektif lazer eritme işleminde, lazerin gücü seçici olarak metali eritir ve bu sıvı eriyik havuzu oluşturur. Lazer o bölgeden geçerken eriyik havuzu aniden katılaşır. Ardışık parçalar tarafından tozların erimesi bir tabaka oluşturur. Bu katmanlar birlikte CAD modelinin verilerine göre katı geometriyi oluşturmak için üst üste birleştirilir. Bitişik tabaka ve parçaların güçlü bir şekilde tutturulması için önceki tabakanın kısmi yeniden eritilmesi ve tarama izinin örtüşmesi yapılır. Bu aynı zamanda, gerekli izotropi derecelerinde daha yüksek bir yoğunlaşma ve tek tip özelliklere yol açmaktadır.

Bu alanda çoğunlukla kullanılan malzemelerden bazıları AlSi10Mg, Ti6Al4V, paslanmaz çelik ve yüksek dayanımlı çeliktir. Bunlardan en yaygın olanı AlSi10Mg'dir. Bu popülerliğin ardındaki sebep onun düşük ağırlığının yüksek mukavemet ve kırılma tokluğu ile birleştirilmesidir. Başlıca uygulama alanı otomotiv ve havacılık mühendisliğidir. AlSi10Mg, Ti6Al4V vb. ile ilgili birçok araştırma yapılmıştır. Maryaşlandırma alanı hala keşfedilmemiş halde iken. Bu, Eİ'de analiz için yüksek dayanımlı çeliğin seçilmesinin nedenidir. Bu tezin amacı, bazı yaygın güç, hız, spot büyüklüğü, penetrasyon derinliği vb. parametreleri dikkate alarak eriyik havuzu şeklini ve boyutunu analiz etmektir.

SLM'de soğutma oranı, ani katılaşma yüksek dayanımlı çelikte iğne martensit oluşumunu kısıtladığı için hızlıdır. Titanyum ve alüminyum birleşik oksitlerin ($Ti0_2$: $A120_3$) daha büyük kalıntıları, 10 ila 20 μm boyutlarında mevcuttur. Bunlar yaşlı

koşullarda mekanik özelliklerin düşürülmesinden sorumludur. Yapısal olarak paslanmaz çelik parça, sünek, düşük karbonlu bir hacim merkezli kübiktir ve martensitik bir yapıya sahiptir. Nispeten daha iyi dayanım ve sertliğe sahip yüksek dayanımlı çelik yaşlandırma sertleşmesi ve yaşlandırma ile elde edilir. Yaşlanma işlemi nikel bakımından zengin metaller arası çökeltileri düzgün bir şekilde dağıtır. Bu çökeltiler martensitik yapının güçlendirilmesinin arkasındaki nedendir. Ve bu çökeltiler aynı zamanda martensitin ostenit ve ferrite geri çevrilmesini de sınırlar.

Katılaşma sırasında uzun taneler eriyik havuzunun merkezine doğru büyür. Epitaksiyel büyüme sadece erime havuzunun merkezi gibi bazı yerlerde görülür. Merkezden uzakta küçük çekirdekli taneler oluşur. Erime havuzunun merkezine doğru birkaç tane parçacık ulaşabilir . Eş eksenli taneler, erime havuzunun tepesinde oluşur. Bir sonraki tarama katmanı, daha önce katılaştırılmış katmanı tekrar eritir ve bu da, eşeksenli tanelerin erime havuzunun üstünden kaybolmasına neden olur. Bu, sadece son eriyik havuzunun üst katmanında değişmeden kalan parçacıklara neden olur .

Bu aşamada eklemeli imalatın performansını etkileyen, tarama hızının artması ile artan ve maximum değere ulaşan yoğunluk gibi çeşitli faktörler söz konusudur. Maksimum yoğunluk noktası farklı tarama hızlarına göre değişir. Tarama hızına karşı yoğunluk, parabolik bir değişim gösterir. Daha yüksek lazer gücü için, düşük tarama hızında minimum düşük yüzey pürüzlülüğüne ulaşır. Erime havuzu sabit kalırsa, yüzey yoğunluğu artan enerji yoğunluğu ile artar.

Genellikle, lazer farklı tarama stratejileri ile uygulanır. Yüzey pürüzlülüğü, gözeneklilik seviyesi, mikro yapı ve ısı birikimi temel olarak tarama stratejisine bağlıdır. Farklı tarama stratejileri tek yönlü tarama, çift yönlü tarama, 2 kat arasında tarama yönünün döndürülmesi, tarama alanını ada taraması olarak adlandırılan küçük adalara bölmektir.

Oksijen erimiş metal ile yüksek sıcaklıkta reaksiyona girer ve metal oksit oluşturur. Metal oksit, üst ve alt kısımdaki sürekli erime nedeniyle esas olarak kenarlarda bulunur. Katkı maddesi imalatındaki metal oksitlerin çoğu, kırılmaları zor olduğu Alüminyum'da bulunur. Oksijen ve oksit oluşumunun sıkışmasını önlemek için, oksit tabakasını önceki katman üzerinde eritecek yüksek sıcaklıkta ısı kullanılması tavsiye edilir. Daha iyi tarama stratejileri ve tarama parametresi, Argon gibi soygaz kullanımı, oksit oluşumunu önemli ölçüde kontrol edebilmektedir.

Birim uzunluktaki P / v başına düşen enerji arttırılarak erimiş havuz hacmi daha fazla büyür ve viskozite düşer. P / v azalırken geri tepme basıncı belirginleşir ve tarama izlerini bozar. Verilen tarama hızı enerjisini daha fazla arttırmak suretiyle tozu tamamen eritmek ve ilk katmanı kısmen eritmek için yeterli değildir. Bu, kararsızlık ve damlacıkların oluşumu ile sonuçlanır.

Tarama hızı arttıkça göreceli yoğunluk azalır. Bu azalma düşük tarama hızında önemli olmamasına ragmen yğunluktaki bu azalmanın nedeni, birim alan başına sağlanan enerjinin lazer tarafından azaltılmasıdır. Çeşitli analizler, katman kalınlığının 30 um ila 40 um arasında arttırılması, yoğunluğun çok az azalırken tarama süresinde % 25 azalma oluştuğunu göstermektedir. Tarama hızını çok düşürerek, tamamlanmamış erime nedeniyle yoğunluk azalır.

Bu tez çalışmasının temel amacı, maraging çeliği kullanılarak eklemeli imalatla elde edilen parçalarda ergimiş havuzun modellenmesi, sıcaklık profili tahmini, maksimum sıcaklık ve ergimiş havuzun derinliğinin tahminidir. ANSYS analiz yazılımının APDL

kısmı kullanılarak çalışma ve simülasyon yapılmıştır. Analize başlamadan önce elastisite modülü, young modülü, yoğunluk, başlangıç sıcaklığı, ısıl iletkenlik, özgül ısı, ısıl genleşme katsayısı vb. gibi özellikler, kullanıcı arayüzü veya ANSYS kodları kullanılarak yazılıma girilir. Girdi verilerine dayanarak, problem çözülmekte ve sonuçları görüntülemek, gerekli grafikleri çizmek için daha sonraki işlemler yapılmaktadır.

Bu çalışmada PLANE55 ve SOLID70 olmak üzere iki tip malzeme seçilmiştir. PLANE55 sürekli hal ya da geçici ısıl analiz ve her bir düğümünde tek bir serbestlik derecesi için tasarlanmıştır. Bu analizler aynı şekilde SOLID70 (Şekil 9.2) için, 3D olarak uygulanmıştır. Bu analizin yapılması için model olarak küçük kübik bir şekil seçilmiştir. Modelin boyutları x = -0.6e-3 mm, y = 1.25e-3 mm, z = -0.8e-3 mm olarak seçilmiştir.

Analizi ANSYS programında yapabilmek için modeli daha küçük parçalara bölmemiz gerekir. Daha küçük parçalarla analiz yapılmasının temel sebebi analizin daha verimli, doğru ve mikro ölçekte yapılabilmesidir. Gövdeye uygulanan yük tüm parçalara dağıtılarak her parça için analiz yapılmıştır. Problemin çözümünde doğruluk ve hız parçalamaya bağlıdır. Bu analizde multizon metodu kullanılmıştır. Bu metot verilen sekli küçük küplere ayırarak uygulanır. Küçük parçalar analiz için daha fazla süre gerektirir. Zaman tüketimini azaltmak için çalışmamızı çok ilgilendirmeyen yerlerde büyük parçalar kullanılırken çalışacağımız bölgede küçük parçalar kullanıldı. En fazla 39401 nokta oluşurken 36818 parça oluşmuştur. Analiz yalnızca 3 katman için yapılmıştır çünkü daha fazla katman ile analiz yapılması çok fazla zaman harcanmasına sebep olacaktır.

Bu durumda 80, 100, 120 W güç girdisi değerleri, 400, 600, 800, 1000 mm/s tarama hızları icin seçilmiştir. Bir katmanın kalınlığı 30 μm'dir. Gönderilen lazer ilk birkaç katmana nüfuz edebilmiştir. Toz tabakası üzerine lazer geldiğinde, daha önce oluşturulmuş tabakanın yanı sıra toza belirli bir derinliğe kadar nüfuz eder. Bunun sonucunda daha önceden oluşmuş toz katmanı tekrar erir ve yaklaşık 3 katman kalınlığında eriyik havuz oluşur. Bu sebeple bu çalışmada nüfuziyet derinliği 100 μm olarak alınmıştır. Lazer çapı 100 μm olarak alınmıştır.

Yüksek dayanımlı çeliğin özellikleri sabit olup sıcaklıkla değişmez olarak kabul edilmiştir. Analiz sırasında sıcaklığa bağlı değişen özellikler dikkate alınmıştır. Eriyik havuzunun şekil, boyut ve sıcaklık dağılımı Şekil 9.10 ila 9.15 arasında gösterilmiştir. Analizin yapılması çok fazla zaman harcanmasına sebep olacağı için yalnızca 3 katman için yapılmıştır.

Sıcaklık ve eriyik havuz davranışı; 3 katman ile güç ve hız kombinasyonu için simüle edilir. Tablo 9.12, elde edilen sıcaklığı ve güç hız kombinasyonuna dayanan eriyik havuz derinliğinin simulasyon sonucunu gösterir. Eriyik havuz derinliğinin yanı sıra katmanlara karşı sıcaklığın sonuçları çizilmektedir. Şekil 9.10 ile Şekil 9.12, sıcaklık davranışını gösterir. Şekil 9.13 ile şekil 9.15 e kadar olan şekiller ise eriyik havuz derinliğinin davranışını gösterir. Daha fazla katman eklenerek sıcaklık ve eriyik havuz derinliğinin arttığı saptanmıştır. Ayrıca bunların her ikisi de hızın artmasıyla azaldığı belirlenmiştir. Bunun nedeni, diğer parametreleri sabit tutarken hızı artırarak mevcut birim hacim başına enerji değerindeki düşüş olabilir.

1. INTRODUCTION

According to ASTM the definition of additive manufacturing is ‘‘a process of joining materials to make objects from 3D model data, usually layer upon layer, as opposed to subtractive manufacturing methodologies. There are many synonyms of additive manufacturing such as additive fabrication, additive processes, additive techniques, additive layer manufacturing, layer manufacturing, and freeform fabrication’’. This definition is mainly applicable to all kinds of substances inclusive of polymer, metal, ceramic, composites etc. Additive manufacturing is in use over for 2 decades to produce small quantity mainly prototypes, it has very recently emerged as a mainstream manufacturing technology which is applicable to most fields of manufacturing and become viable for commercial use.

The usage of Additive Manufacturing (AM) is very recently expanded with most of the major companies located in the vicinity of Europe and nearby. It is now possible to manufacture complex metallic geometries and the process is not only restricted to prototypes. Additive manufacturing is now making a revolution in most of the manufacturing companies for example automotive, aerospace industry, energy sector, medical instruments and tooling (Figure 1.1).

Figure 1.1 : Gas turbine manufactured by Selective Laser Melting.

There are many technologies of the additive manufacturing of metals, so there are many synonyms of it as shown in graph below. Most common name (Figure 1.2) in industrial market is additive manufacturing but the mainly used term in consumer market is 3 D printing [1].

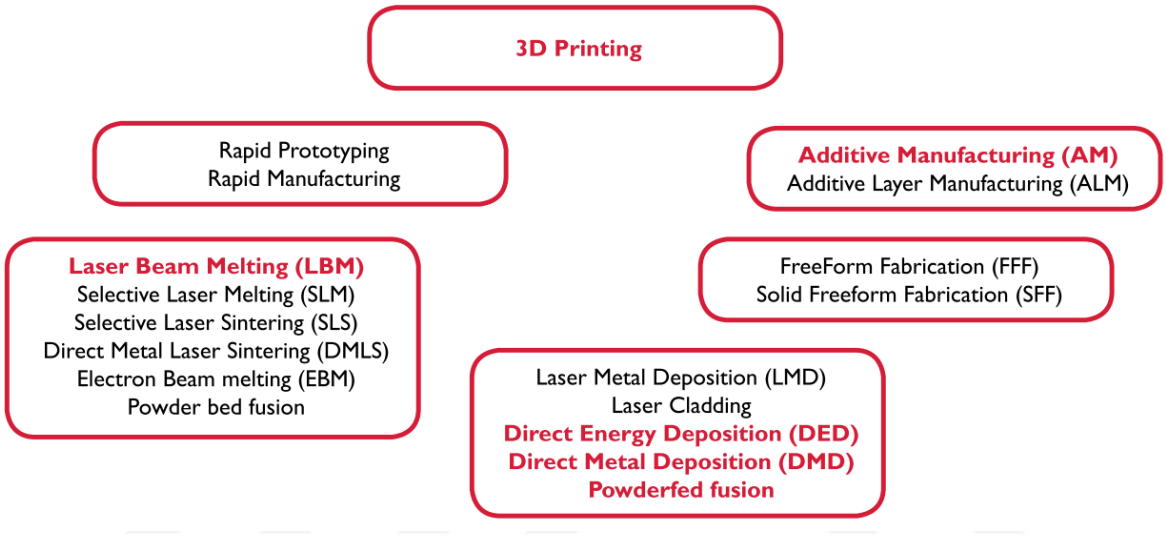

Figure 1.2 : Synonyms and classification of additive manufacturing.

1.1 The Advantages of Additive Manufacturing

Following are some advantages of additive manufacturing

- Here is more freedom of design as compared to casting and machining
- Very low weight parts are possible to manufacture by designing by supplying material where is it needed without other places.
- Very complex internal design with several parts simultaneously possible.
- As additive manufacturing design parts very near to net shape of final product, it consumes 24 times less material as compare to machining which is very important if material is very costly or complex in machining. It possible to manufacture complex part in a single pass which eliminates the secondary operations of assembling like welding, brazing and soldering.

- No requirement of tool as compare to other processes such as casting, machining etc.
- Very short production time, the time for production of highly complex parts varies from minutes to few hours where parts are fabricated layer after layer. The cycle time is very low as compare to conventional manufacturing system. In additive manufacturing the cycle time varies from few days to weeks whereas in other process it usually takes several months [1].

Below are some examples of complex design made by additive manufacturing, which may not be possible by other conventional method of manufacturing.

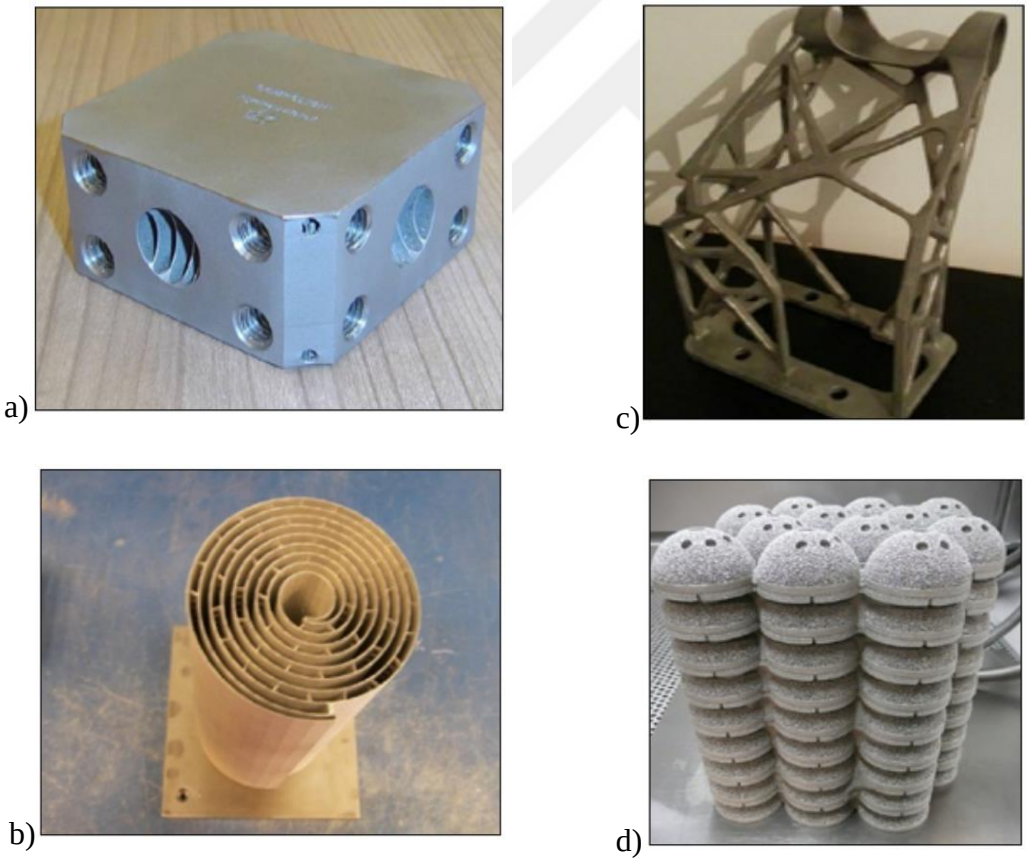

Figure 1.3 : (a) Hydraulic prototype, (b) LBM fabricated Prototype, (c) Support of satellite, (d) Ti6Al4V implant with particular surface design.

1.2 The Disadvantages of Additive Manufacturing

To make benefit from advantages of additive manufacturing, it's better to consider the disadvantages too:

- Product size: Most of the time the standard dimension of powder bed in powder bed technology is 250x250x250 mm, so the maximum size of part produced cannot cross this dimension. But in process such as direct energy deposition (or laser metal deposition) greater part size can be produced. But because of thin powder layers, the process is very slow and cost more in fabricating high or massive products.
- Production size: The additive manufacturing is generally feasible for small and critical design batch of products and is not suitable for mass production. Research and efforts are going on to increase productivity as well as production of large size parts. Additive manufacturing already producing small size parts with quantity of approximately 30000 parts a year.
- Designing: When overhanging angle is less than 45^0 removable support structures are needed for in powder bed technology.
- Material: Every metal is not being able to produce by additive manufacturing but limited to easy to weld materials. And hard to weld materials need particular approach, change of parameters.
- Properties: Product produced by additive manufacturing have an anisotropy in the direction of fabrication.
- It is possible to have some porosity in spite of the fact that 99.9 percent density can be reached by this process. Properties are better than casting parts but lower than wrought parts [1].

1.3 Market Perspective and Application

The growth of industries like aerospace, food, manufacturing, automotive and health care are demanding the commensurate growth in additive manufacturing technologies [2]. An appreciable high demand can be expected from medical and dental sector till 2025. The consumption and per capita income is expected to grow in near future leading to economic

growth and hence the demand for emerging technologies such as additive manufacturing. Furnished goods and design parts will be mainly utilizing additive manufacturing technologies in near future.

In mainstream various companies, institutes and organizations are effecting the market progress of additive manufacturing. Big companies are putting money into research and development such as HP originally a printing business company are trying to enter the additive manufacturing vast market. Educational and research organization are allocating funds for research and development activities like European Union's Horizon 2020 program.

Universities are collaborating with industries to create research and innovation centers, for example Advanced Remanufacturing and Technology. Now there is a boom in the market for additive manufacturing as not much research work has been done. The stakeholders are trying to explore the untouched part of additive manufacturing and new industries are trying to put their foot in this area.

At present the use of additive manufacturing is high in mostly developed countries, but its use is very limited in developing countries. The additive manufacturing market is expected to reach double digit growth in CAGR for the forecast period. There are three major geographical regions for the popularity of additive manufacturing.

- Middle East & Africa,
- Japan,
- Asia Pacific Excluding Japan,
- Western Europe, Latin America,
- North America.

The other regions such as western Europe and north America also registered and appreciable growth in the worldwide additive manufacturing market (Figure1.7).

In 2018 the total market acquired by additive manufacturing is nearly 12.8 U.S. billion dollar. Worldwide market value of 3 D printing is estimated to expand at CAGR of nearly 18 to 22 percent in a forecast period of 2015 – 2018. The reason is the high demand from biggest industries such as dental, medical, automotive, health sector and manufacturing.

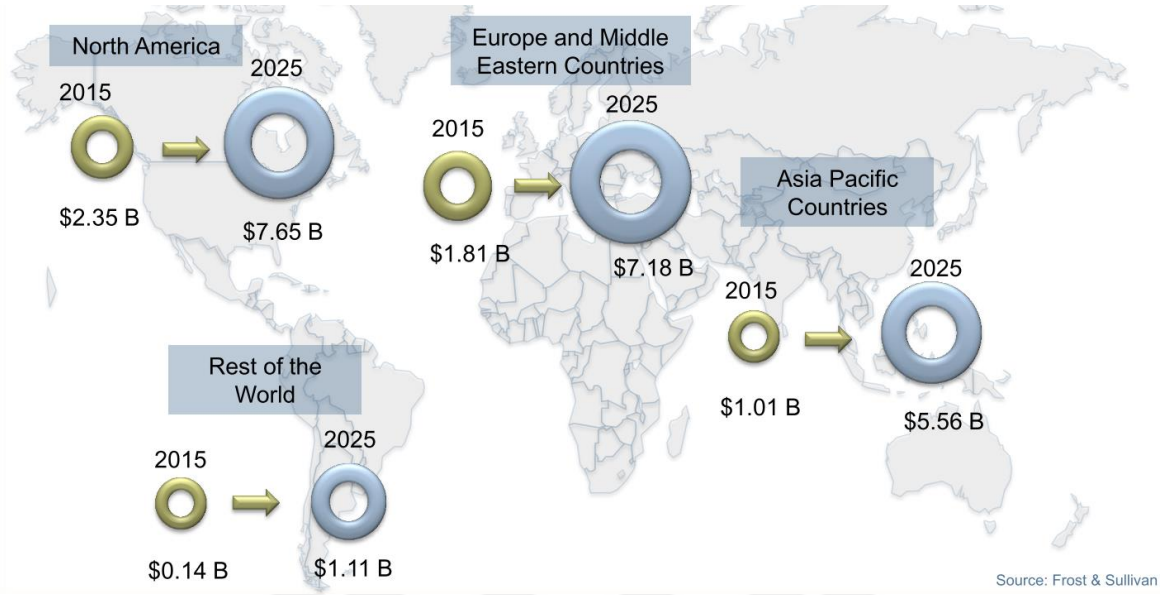

Figure 1.4 : Region wise revenue generation from 2015 to 2025.

The U.S. is among the leading innovator and initiator in adopting of additive manufacturing and is estimated to maintain this position as a market chief in the forecast period. During 2016, U.S. patent and trademark office confirmed that additional 8000 patents were registered in the area of additive manufacturing related materials. The variety of patents varies from household items to prosthetic kits and consumer products. The invention of 3 D bio printing is believed to have a positive growth in U.S. economy, with all businessman and industrialists hoping to take advantage of 3 D printing technology.

1.3.1 New initiatives in the market

In December 2017 a company General Electric Co, has declared that it will increase its share in Swedish 3 D printer maker Arcam AB ARCM.ST to nearly 95 percent which was 77 percent before after purchasing shares from hedge funds Elliot and Polygon. General Electric Co announced that it can by Elliott Management and Polygon Investment Group's shares of 345 Swedish crowns ($41.44) each.

In 2017 Materialise NV reported that it has agreed with Siemens' product lifecycle management (PLM) software business, to assist for design a seamless process for design

and manufacture of parts using 3 D printing technology. From this deal both the companies will be working together in order to make compatible Materialise's AM software technologies with Siemens digital solutions

Singapore Economic development board has recently invested $500 Million for foster their countries additive manufacturing sector for the upcoming 7 years. National technological university (NTU) has invested USD 30 Million for fabricate an additive manufacturing center and has also constructed and assembled additive manufacturing driven startup [3].

Chinese ministry of industry and information technology just launched its last longing plan for additive manufacturing. Additive manufacturing industry in china will going to receive a growth rate in revenues of more than 30 percent a year. Chinese government has planned to inaugurate 2 to 3 globally competitive additive manufacturing companies. Below figure Figure 1.8 shows the market share of main countries

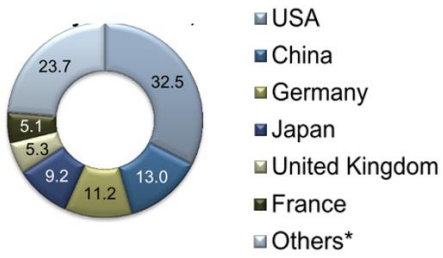

Figure 1.5 : Percentage of market share of various countries around the world in 2015.

Some of the major companies in additive manufacturing markets are

- Materialise NV
- 3D Systems, Inc.
- MCor Technologies Ltd.
- ExOne
- EOS and Stratasys Ltd.
- HP Inc

- Nano Dimensions
- Organovo
- Proto Labs
- Stratasys
- SLM solutions group
- Voxeljet

1.4 Applications of Additive Manufacturing

Following are the different applications of additive manufacturing.

1.4.1 Medical application

There are many experiments which are successful in laboratory but still it needs an arduous journey to explore fully and reach the target in field of medical. Blood vessels, bones, cartilage and skin are successfully generated in the laboratory utilizing additive manufacturing technology. Each of these processes are done using micro scale ultrafine layers.

The notable work is done by the generation of progenitor cells which can morph into different categories of cells. Kidneys, bones, ears and bladders can be generated with precise dimensions, quality and desired characteristics (Figure 1.9 and 1.10). Generation of body parts need arduous effort, profound skills and great care.

Figure 1.6 : A human skin generated from 3 D printing using stem cells.

Skin can be very easily generated with this technology while completely solid organs like heart are very difficult to fabricate [4].

Customized tools and surgical instruments are already producing since many years by additive manufacturing. 3 D printing also become popular in dentistry, for fabricating moulds for casting parts for implanting.

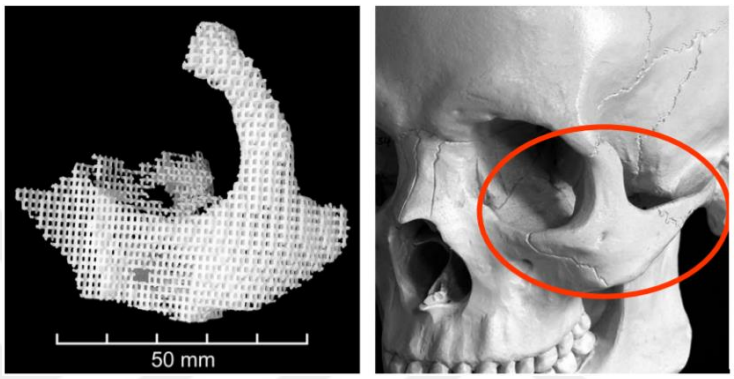

Figure 1.7 : Damaged part of skeletal replaced by AM part.

1.4.2 Aerospace and defense sector

The use of additive manufacturing in aerospace and defense industries has been grown to 26 percent CAGR (2015-2025). The cost of manufacturing and time are decreased by at least 10 times for producing low quantity and complicated parts.

- Some of the basic examples are turbines (Figure 1.8) inlet valves and nozzles.
- Wing spare parts, hinges, air ducts and complex parts of jet engines are manufactured by additive manufacturing in aerospace industry

In defense industry and for low volume production EBM is perfectly suitable. Because the multiple parts can be produced in single times so additive manufacturing has led to the shrinkage of manufacturing chain.

1.4.3 Automotive

Companies like local motors and Cincinnati incorporated have manufactured car wholly by 3 D printing. The car body is made up of carbon fiber and it took 48 hours to fabricate a car with 212 layers. BMW has fabricated hand tool by 3 D printing for automobile assembly and testing (Figure 1.9) [3]

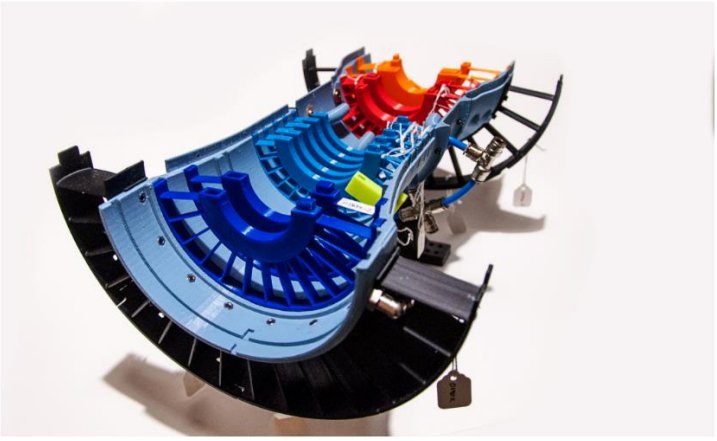

Figure 1.8 : A model of jet engine built by AM.

Figure 1.9 : BMW car and hand tool manufactured by AM.

2. LITERATURE REVIEW

Temperature profiles, energy absorption, microstructure, deposit geometry, temperature profile are effected by the energy absorption by materials. Energy absorption varies with heat source features. Density distribution of power of laser beam, electron beam and plasma arc follows axisymmetric Gaussian profile and is given by

$$P_d = \left(\frac{fP}{\pi r_b^2}\right) exp\left(\frac{-fr^2}{r_b^2}\right) \tag{2.1}$$

Here f is the distribution factor, r_b is the heat source radius, r is the location of point of interest from heat source, P is the net power of heat source. A higher value of f refers to the high power density of source axis, and a high value of r_b refers to the lower value of power density at all location of heat source. Figure 2.1 shows the density distribution of heat source with various values of distribution [5].

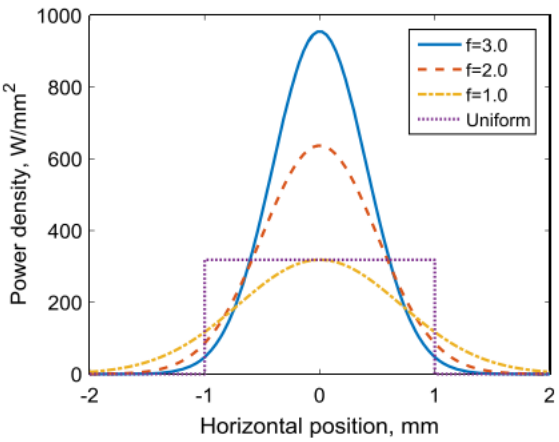

Figure 2.1 : Density distribution with varying value of f.

With higher value of f, the power density is more concentrated at center, while at higher values of r_b its more distributed throughout [6].

2.1 Interaction of Heat Source with Powder

The interaction of heat source with powder may be in 1 step or multiple, totally dependent on the nature of process. For example, in direct energy deposition process (DED), partial

heat is absorbed by powder as they ejected from the feeding nozzle. The heat absorbs depend upon density, properties, size and shape distribution, gas velocity, duration of travelling etc. During the travelling the powder particles are heated to a temperature below the melting point [7]. The heat source in a DED process is a modified Gaussian distribution and can be expressed as

$$P_d = \frac{fP}{\pi r_b^2 t_1}[\eta_P + (1-\eta_P)\eta_1]exp\left(-f\frac{r^2}{r_b^2}\right) \quad (2.2)$$

Here η_p represents the portion of energy absorbed on the way after ejection, η_1 is the absorption coefficient and t_1 is the layer thickness of powder. The value of absorption and hence η_1 ismaximum during solid form of powder, but its value reduces as the liquid surface is formed. During liquid surface the absorption of energy takes place by Fresnel absorption.

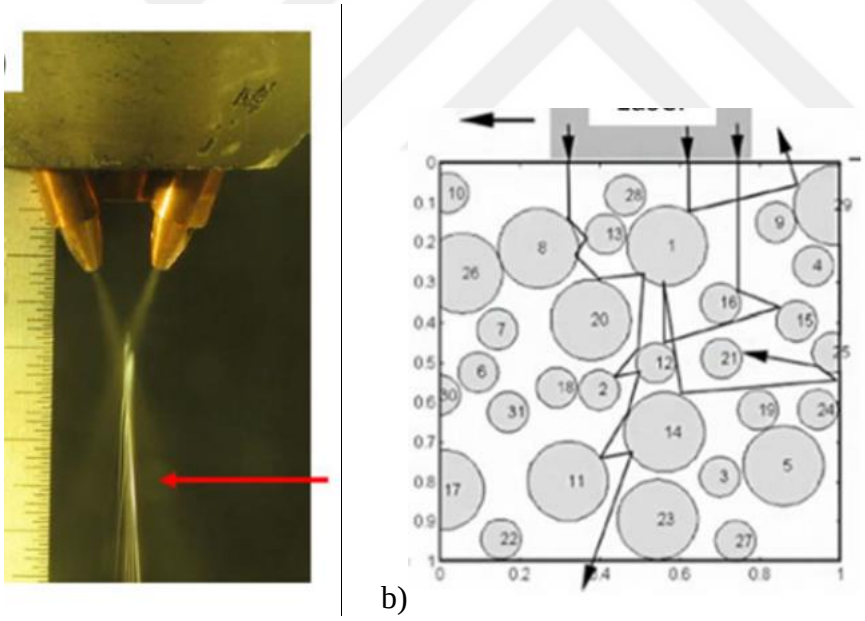

a) b)

Figure 2.2 : Interaction of laser with powder (a) after ejection for DED (b) In powder bed.

In powder based fabrication process, the whole energy is directly reached to powder bed. After the laser energy hits the powder bed, some part of energy is absorbed by powder, some is reflected until it comes out of powder or its value become negligible (Figure 2.2). Heat absorptions is dependent on powder properties such as size, material properties, packing density etc. [8].

2.2 Mechanism of Heat and Mass Transfer

The flow of liquid metal results in mixing, and leads to the transportation of heat in the molten pool as shown in figure 2.3 below

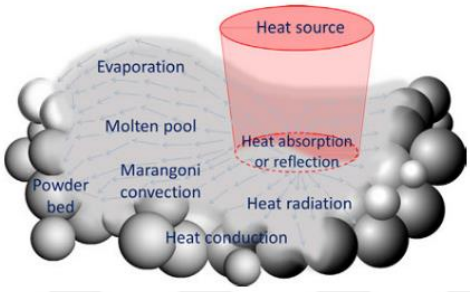

Figure 2.3 : Mechanism of heat transfer.

Temperature distribution in molten alloy, heating rate, cooling rate, microstructure, properties and solidification pattern are affected by calculation pattern. So the calculation of temperature requires couple solution of fluid flow and heat transfer equation. For easy convergence of solutions, some simplifications are made like densities of liquid and solid form are assumed constant, layer deposition surface is flat, vaporization of alloying elements induced thermal effects are kept constant since these assumptions does not significantly affect the solution[9].

The temperature distribution can be achieved from the equation of energy, momentum and mass [10].

$$\frac{\partial(\rho u_i)}{\partial x_i} = 0 \tag{2.3}$$

$$\frac{\partial(\rho u_j)}{\partial t} + \frac{\partial(\rho u_j u_i)}{\partial x_i} = \frac{\partial}{\partial x_i}\left(\mu \frac{\partial u_j}{\partial x_i}\right) + S_j \tag{2.4}$$

$$\rho \frac{\partial h}{\partial t} + \frac{\partial(\rho u_j h)}{\partial x_i} = \frac{\partial}{\partial x_i}\left(\frac{k}{C_p}\frac{\partial h_i}{\partial x_i}\right) - \rho \frac{\partial \Delta H}{\partial t} - \rho \frac{\partial(u_i \Delta H)}{\partial x_i} \tag{2.5}$$

Where, i, j are directions u_i and u_j are velocity components, ρ is the material density, t is time x_i is the distance along i direction, S_j stands for source term, μ is dynamic viscosity, C_p is specific heat, ΔH is latent heat, k is thermal conductivity. The term S_j is applied during arc or electron beam and considers the effect of electromagnetic and buoyancy

forces. The solution of this equation gives the temporary temperature distribution in full body and velocity distribution in molten regions, solidification parameters, cooling rates[11]. These equations can be solved using situations at border.

2.3 Boundary Conditions

Marangoni flo is defined as the gradient of surface tension at the melt pool. Which directs the travelling pattern of molten metal. This can be defined as

$$\tau_m = \frac{d\Upsilon}{dT}\frac{dT}{dr} = -\mu\frac{du_i}{dx_k} \tag{2.6}$$

Where Υ is surface tension, T_m is stress from Marangoni effect, u_i is velocity component in I direction, x_k is distance along k direction (vertical). This stress is responsible for the travelling of metal in fusion zone [12].

Component of velocity perpendicular to the surface and meeting point of solid liquid are assumed to be 0. The transfer of heat at the surface of the built part and surrounding is based on convective as well as radiation transfer of heat and can be expressed as

$$-k\frac{\partial T}{\partial z} = \sigma_{SB}(T^4 - T_a^4) + h_c(T - T_a) \tag{2.7}$$

Where, T_a is ambient temperature, ε is emissivity, σ_{sb} is Stefan Boltzmann constant, h_c is convective heat transfer coefficient [13].

2.4 Role of Non-Dimensional Numbers

These numbers are effective in estimating the influence of different additive manufacturing parameters on properties, microstructure and defects. These are favourable in the context that, they combine the effect of various parameters in 1 single non dimensional number and able to provide much insight which a single parameter cannot. Like the significance of transfer of heat via conduction and convection in pool can be evaluated by Peclt constant Pe. If a Pe >>1, which is a high value indicates that convection is the main cause of heat transfer in melt pool [14].

Marangoni number Ma is the proportion of surface tension force to viscous force. This number represents the strength of flow of liquid metal by convection in the melt. The shape of melt pool depends on the value of Marangoni number which is determined by surface tension gradient in the pool.

Fourier number F_o is the ratio of heat dissipation to heat storage rate in additive manufacturing process. High value of F_o represents higher heat dissipation resulting faster cooling rates and hence more refined microstructure [15].

3. CLASSIFICATION OF ADDITIVE MANUFACTURING

Additive manufacturing process can be classified on the basis of heat source used or on the basis of powder application mechanism.

3.1 Based on Heat Source Used for Additive Manufacturing

In laser beam melting a laser of nearly 100 µm spot size diameter melts the top powder layer of the substrate. The lase is partially absorbed, partially scattered, and partially reflected by powder particles (Figure 3.1). Laser power typically ranges from 200 Watt to 1000 Watt.

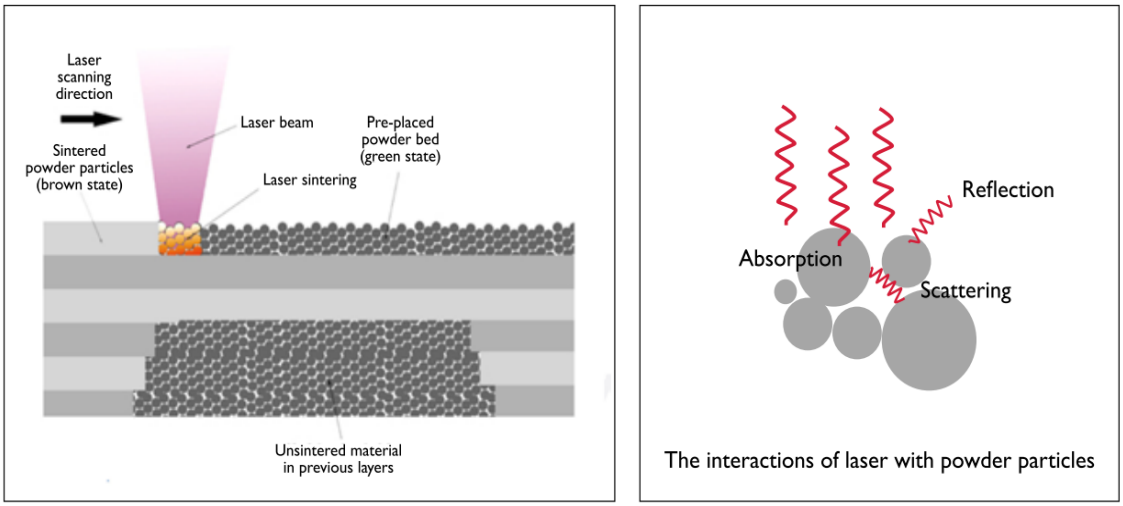

Figure 3.1 : Process of additive manufacturing.

Within a single layer the laser is applied multiple times to melt the whole area of layer. The laser can be applied in different strategy and patterns with variable hatch spacing, spot size, overlap to attain the needed temperature, density, to avoid porosity.

The additive manufacturing process is divided by source of heat and method by powder application. In beam based systems either electron beam melting of laser beam melting, initially powder is applied at platform then laser or electron melts the powder selectively.

The platform is lowered and process is repeating again and again until the desired product with required thickness is achieved. The additive manufacturing process can be

- Laser beam melting
- Electron beam melting
- 3 D printing
- Direct energy deposition (Laser metal deposition)

The following discussion will elaborate each of these methods

3.1.1 Laser beam melting (selective laser melting)

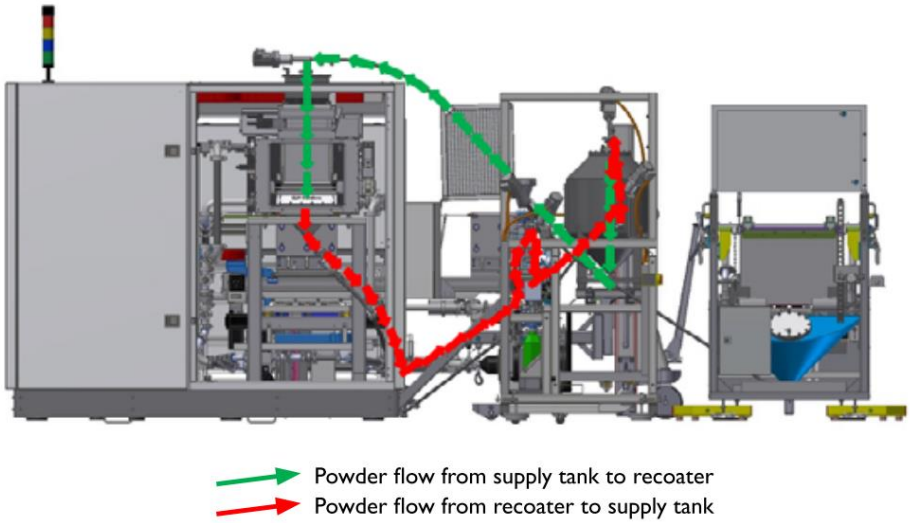

Figure 3.2 : SLM machine with flow directions (by SLM solutions).

SLM is a type of 3 D printing process where parts are created layer by layer (a setup is shown in figure 3.2 and 3.3). CAD data of the part is converted to a format which can be used by additive manufacturing machine. The powder is applied at platform with re coater. The laser than scan area of powder according to shape of part to be produced in that layer. Laser melts the portion of powder layer and completely fuses the powder particles. The platform is the lowered up to 100 µm[1]. The process is repeated layer by layer and each successive layer fuses with other in order to from the final product. The maximum powder bed size of SLM machine is 500 mm. Density of nearly as cast part can be achieved by

this process. Almost no post processing is needed except surface finishing. Figure shows the schematic view of additive manufacturing [16].

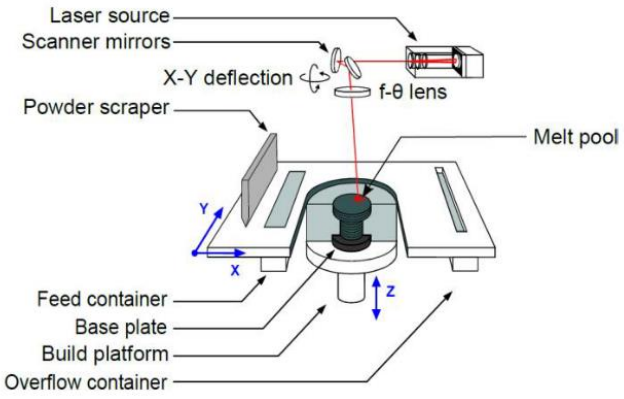

Figure 3.3 : Interior view of SLM machine components.

In conventional sintering the powder particles bond together without complete melting. This process can be possible in 2 ways, either in solid state known as solid state sintering of in partially liquid state known as liquid phase sintering.

The solid state sintering occurs at a temperature lower than melting. At high temperature, the powder moves slowly to contact region of nearby particles and forms a sharp angular pore. After this initiation more particles move into that region and forms a neck between adjacent particles (Figure 3.4).

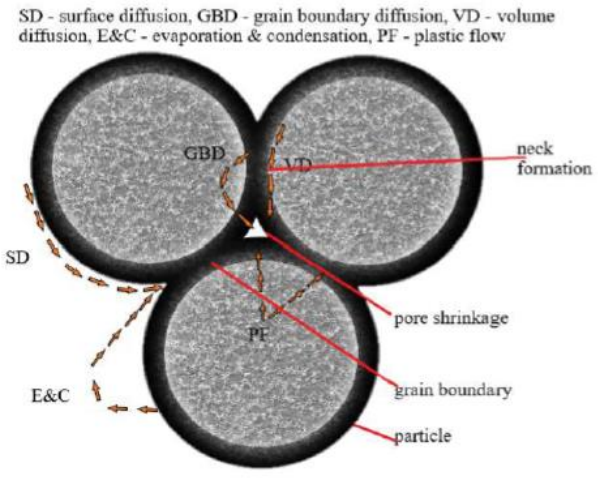

Figure 3.4 : Mechanism of powder diffusion in SSS.

There are several mechanisms involved in the migration of particles at the pores like diffusion from grain boundaries known as grain boundary diffusion, volume diffusion and surface diffusion. The movement also take place by evaporation at other regions and condensation at neck area. Majority of particles movement takes place by volume diffusion and grain boundary diffusion.

Liquid phase sintering can be achieved in various ways by using binding material, the method of addition of binder may be in the form of binder grains, combined with structural such as composite grains, grain having a coating of binder, as an alloys with different melting temperature of metals. Mostly the interior of surface remains solid while the surface of the grains melts during processing.

In liquid phase sintering the mixture contains 2 types of grains that is a higher melting point metal or ceramic and a lower melting point binder. During process the material is heated to a temperature between liquidus. The binder becomes liquid while metal/ceramic remains in solid state resulting in consolidation of part.

The densification of part is dependent on the 3 simultaneous stages particle arrangement, solution precipitation, solid state sintering. Due to very short interaction of laser with material only particle rearrangement is responsible for densification in solid laser sintering process. In SLS high density and metal bonding is dependent on packing of powder particle.

The mechanism of SLM is same as SSS only that the higher power is used in complete melting of powder in SLM. SLM produced parts have comparatively enhanced microstructural as compared to SSS.

3.1.2 Electron beam melting (EBM)

Electron beam melting is process that reduces time, weight and cost simultaneously. In this process the kinetic energy of the electron travelling with speed approximately half of speed of light is converted to thermal energy after striking the powder (Figure 3.5). This conversion of energy results in rise of temperature above melting point. In electron beam a tungsten filament heats the electron.. The process is 4 times faster than other additive manufacturing process. This process is 5 to 10 times more efficient than laser technology.

The parts produced by this process are free from the residual stresses. The process is carried out in vacuum and preheating of powder before melting[17].

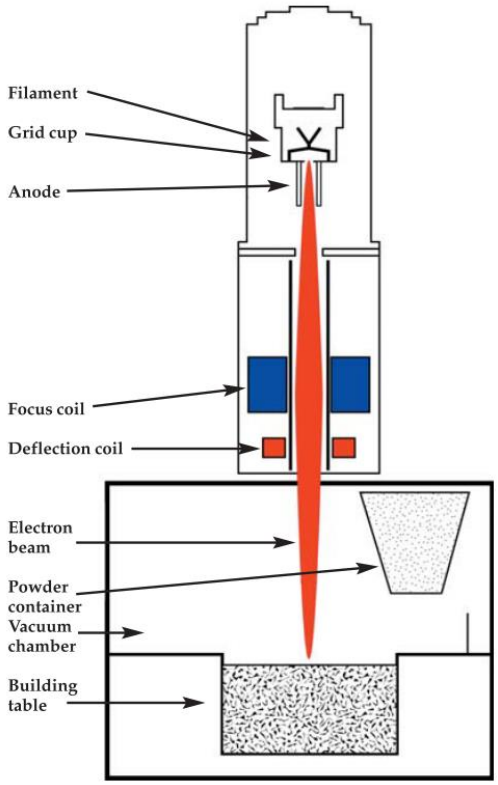

Figure 3.5 : Schematic diagram of electron beam melting main components[17].

3.1.3 3 D printing

In 3 D printing is similar to SLM and EBM except that instead of supplying energy through the nozzle a binder is supplied. The powder layer is applied on the built platform with the help of roller. The binder applied through the nozzle in the specific area. Again a powder layer is applied and binder binds the powder. In this the part from is in the green form so care is needed in order to remove the part from built platform.

In the following stages sintering and debinding process takes place. This technique has better productivity as compared to LBM. No support structure is needed in this process as there is no melting of parts. The mechanical properties are inferior to LBM and EBM with application to very limited materials [1].

3.1.4 Direct energy deposition (laser metal deposition)

DED is used for repairing, rebuilding of damaged components, manufacture of new parts and to apply corrosion resistant coatings. This process can produce fully dense parts by adding material pixels by pixels using CAD data. This process is a closed loop feedback system, which keeps in maintaining material integrity and dimensional accuracy. In this process it is possible to adjust the laser power automatically from the feedback of temperature of melt pool. Real time composition monitoring is done by spectroscopic analysis [18].

A nozzle deposits melted material on the base where its solidifies. The productivity is high as compared to LBM and EBM.

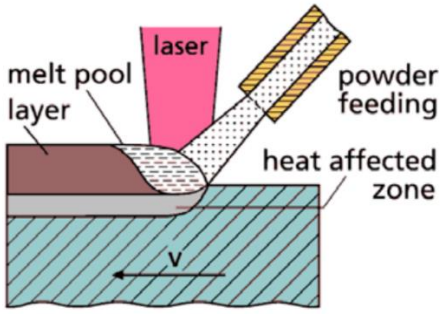

Figure 3.6 : Direct metal deposition process.

4. MATERIALS FOR ADDITIVE MANUFACTURING

The following figure represents the different types of materials and their practical relevance. The shaded ellipse (Figure 4.1) shows the different types of materials developed by EOS and their corresponding area of application. Additive manufacturing covers a broad range of materials. These will be shown in the following section [19].

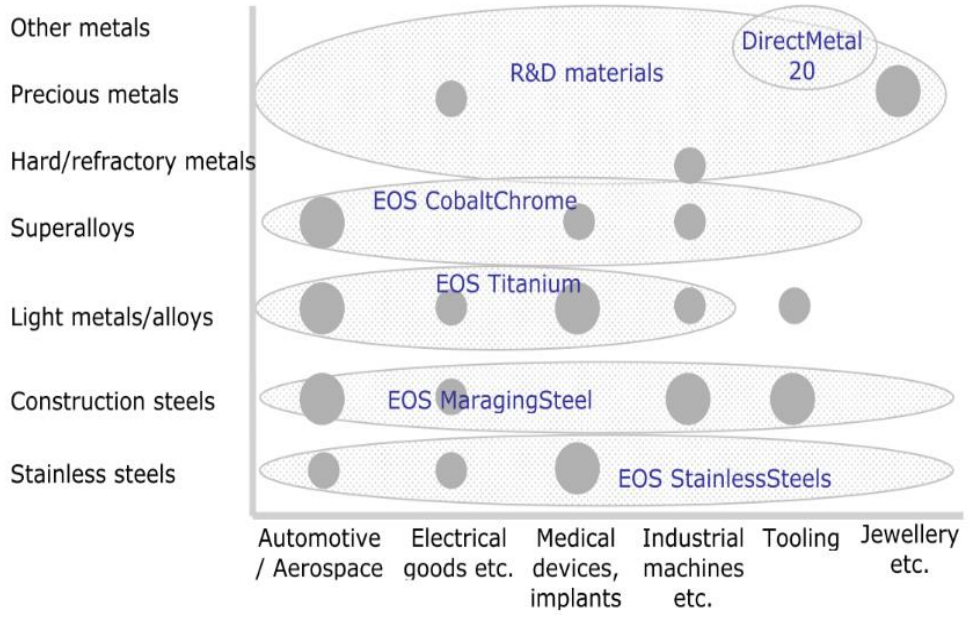

Figure 4.1 : Materials for AM developed by EOS and their area of application [19].

4.1 Non Standard Materials

Direct Metal 20 is bronze nickel based material can process a thickness low up to 20 µm. Using this material higher building speed can be achieved with porous structure inside the parts with significant strength of the final product. The parts fabricated with this material have excellent resolution, good surface quality, good mechanical properties and can be easily polished. Their primary applications includes inserts for injection moulding and functional metal prototype [20].

4.2 Stainless Steel

The quality of better mechanical properties combined with excellent corrosion resistance at low cost, steel is widely used in every sector of engineering. Some commonly used stainless steel which are also applicable to additive manufacturing are StainlessSteel GP1, whose composition corresponds to European 1.4542. Its tensile strength is nearly 1000 MPa with 25 % elongation. Another grade of steel developed by EOS is EOS StainlessSteel PH1, whose composition corresponds to European 1.4540, whose yield strength (1300 Mpa approx) and hardness are superior to Stainless Steel GP1. They can be used to manufacture medical instruments, small products, prototypes, spare parts etc [21].

4.3 Construction and Tools Steel

A wide range of construction cast and tools steel are available. EOS selected EOS Maraging steel MS1. This is ultra-high strength steel and its chemical and physical composition is according to to US classification 18 Maraging 300. This steel have a very high strength of 1900 MPa, hardness of 55HRC approximately with a very high toughness. This type of steel is used for very high performance industrial applications like inserts for moulds whose life can be millions of parts, very high duty injection moulding. It has been reported that MS1 8-cavity series production injection mould having laser-sintered core insert has produced 3 million plastic products [22].

4.4 Super Alloys

These are the alloys which have very high strength and good performance at elevated temperature. Generally, these alloys are nickel or cobalt based [23]. EOS Cobalt Chrome MP1 is a cobalt based super alloy have a ultimate tensile strength of 1150 MPa and hardness of 35 – 45 HRC. MP1 have a very high corrosion and temperature resistance. Its typical application includes turbine blades, cutting parts, accessories of engines. Main medical applications are implants, knee, toe, hip bone etc.

Another type of cobalt based super alloys is EOS Cobalt Chrome SP1. The quality of excellent corrosion and temperature resistance make it a perfect material for dental application [24].

4.5 Light Alloys

The most common types of light alloys used in industries are aluminum and titanium based. Titanium based alloys are difficult to machine and cast so they are very expansive to manufacture. This is the main reason of popularity of titanium alloys in additive manufacturing. However, aluminum alloys can be very easily cast and machined making it a very cheap for manufacturing. EOS Titanium Ti64 is a very popular alloy having excellent mechanical properties as well as corrosion resistance. The hardness and strength of Ti6Al4V manufactured by additive manufacturing is better than as forged part. Its main application includes, engine and structural components for aerospace, biomedical and racing implants etc. [25].

4.5.1 Almunium (AlSi10Mg)

Aluminum excellent properties combined with low weight make it among the most popular materials for automotive, aerospace and food industry. It has very good welding properties and hence can be very easily processed by additive manufacturing techniques. According to ISO 3522 the combination of AlSi10Mg alloy is given in table 1.1 below[16]

Table 4.1 : Composition of AlSi10Mg [26].

Element	Al	Si	Cu	Mn	Mg	Zn	Fe
Weight (percent)	rest	9-11	<0.1	0.05	0.45-0.6	0.05	<0.1

4.5.1.1 Powder morphology of AlSi10Mg

For better manufacturing of additive manufacturing of part, it is better to compare the powder characteristics with ISO 3522. The composition of AlSi10Mg powder is given in above table. Lower silicon percentage can lead to less absorption of laser energy and large variation between liquidus and solidus temperature, which will affect solidification of additive manufacturing part [1]. Powder size distribution directly affects the melting behavior [27].

For this 2 kinds of powder are compared from 2 different manufacturers. The SEM image of these 2 types of powder particles is compared as shown in figure 4.2 below. Figure shows that S1 powder more spherical morphology and smother surface.

The powder size of S1 type powder is 16.3 µm while the powder size of S2 powder is 48.4 µm. These characteristics will leads to better flowability and enhanced homogeneous layer of S1 powder as compared to S2[28].

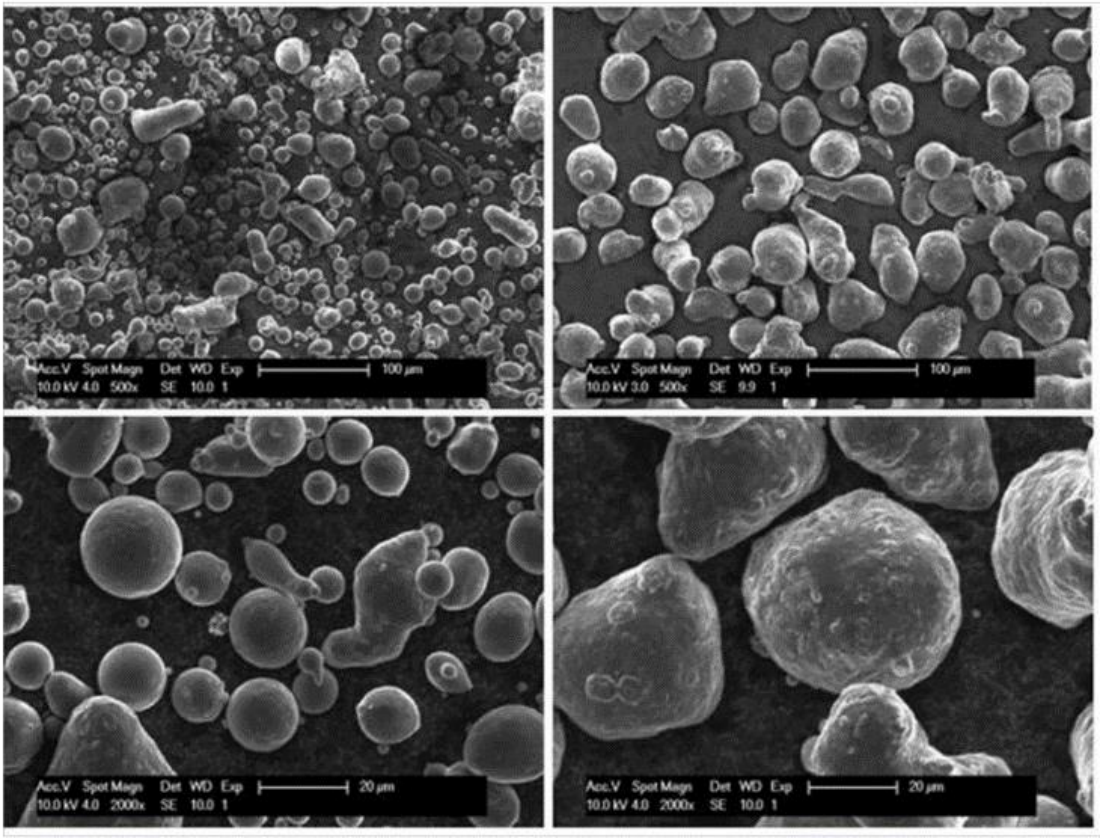

Figure 4.2 : SEM image of powder particles for morphology comparison [6].

4.6 Maraging Steel

Maraging steel 300 (18Ni 300) is iron nickel steel alloys. It is mainly used in land gear, tooling application, rocket motors and aerospace industry where high strength combined with high fracture toughness is desired.

Maraging steel have high dimensional accuracy which makes it perfectly useful for drill chucks, plastic injection moulds, extrusion, tools for punching. Its low carbon content

lowers the possibility of quench cracking. The presence of nickel particles and negligible carbides make its better for corrosion resistance [2].

The high strength and toughness is a result of aging of soft martensite with is formed by cooling of Ni consisting of γ Fe. Strengthening particles like Ni3X (X = Ti, Mo, V, and W) forms during age hardening for short time at temperature ranging from 400 to 450^{o}C [29].

The composition of 18-Ni maraging steel alloy provided by Sandvik Osprey LTD, produced by gas atomization shown in following table

Table 4.2 : Composition of Maraging steel 300 [30].

Element	Ni	Mo	Co	Ti	Al	Si
Weight in %	17.6	5.3	9.6	0.7	0.09	0.2

Mostly the maraging steel powders for additive manufacturing is prepared by gas atomization process. The average particle size is 35 µm. The recommended morphology of good quality additive manufacturing powder is spherical. The SEM image of one such specification of powder shown below in figure 4.3 [31].

Table 4.3 : Commonly used alloys in AM and their chemical composition.

Alloys	Ti	Al	V	Fe	Ni	Cr	Mn	Mg	Si	Mo
SS 361	-	0.005	-	Bal	8.26	17.2	1.56	-	0.33	-
Ti6Al4V	Bal	6.28	3.97	0.052	-	-	-	-	-	-
IN 718	1.02	0.5	-	Bal	53.4	18.8	0.07	-	0.12	2.99
800 H	0.35	0.25	-	Bal	31	20.6	0.85	-	0.32	-
H 13	-	-	1.2	Bal	-	5.5	0.6	-	1.25	1.75
AA6061	0.15	Bal	-	0.7	-	-	0.15	1.2	0.8	-

The spherical morphology results in free flow of powder during additive manufacturing and increases process efficiency.

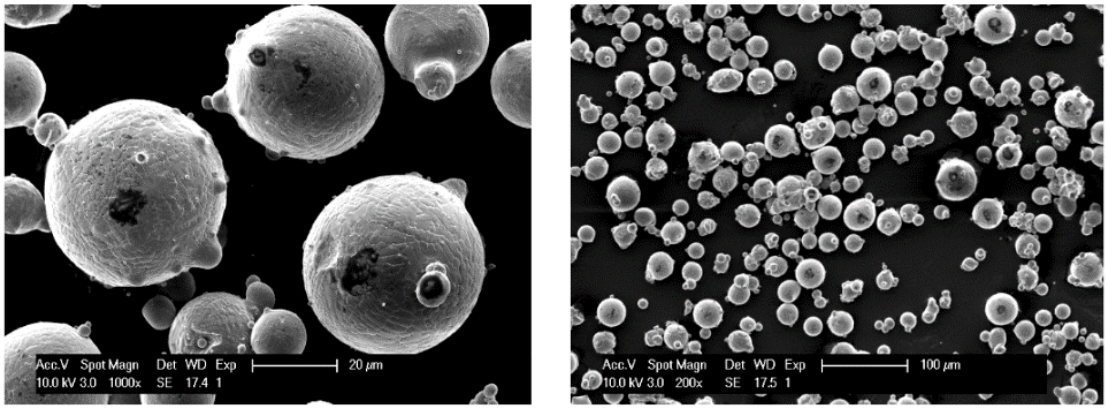

Figure 4.3 : SEM image of maraging steel 300 powder[31].

5. STEPS IN ADDITIVE MANUFACTURING

Additive manufacturing converts the information from computer aided design file to stereo lithography. By doing this the CAD drawing is constructed by triangles and later its take the form of layers, one over another which can be later printed to form 3 D object. The procedure for rapid prototyping for product fabrication is shown in figure below[32].

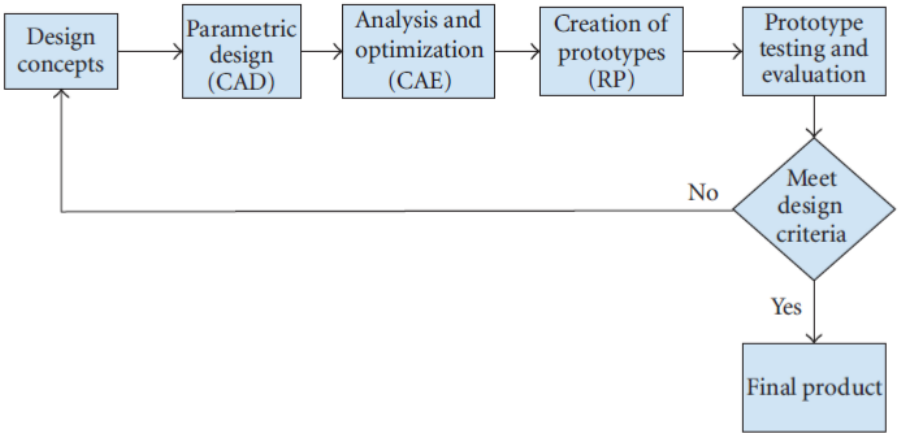

Figure 5.1 : steps involved in rapid prototyping.

The process of rapid manufacturing become possible by the combination of other technologies such CAD, CAM and CNC. Combination of these technologies make possible the printing of 3 dimensional object[33].

Depending on technology, machine and its component the process consists of basic 3 steps. These steps can be combined, expand and change appearance from process to process but the concept will remain similar.

5.1 CAD Model Generation Based on Design

The first step of additive manufacturing is 3 D CAD model, where the imagination and parameter concept takes the virtual form in computer. The information of shape, property

and material can be stored in digital form. Few examples of designing software are solidworks, autodesk, Creo, NX etc.[33].

5.2 Conversion of CAD File to an Acceptable AM File Format

All additive manufacturing technologies to present scenario uses stereolithography (STL) format. Figure 5.2 shows and example of STL file format. STL file format divides 3 D model by stitching triangles of different sizes and captures all the surfaces. Additive manufacturing program determines the location of surface of the part and also the location of interior and exterior of the part from the stored location of triangle and vector normal to the surfaces.

Only shape feature can be saved in STL file and rest of information derived from CAD geometry is ignored. All information related to colour, material, unti etc which plays a vital role in fabrication of material is ignored while transforming the part. The "AMF" file format is recently developed to overcome the limitations and now it is an ASTM/ISO standard format. That can also store material, color and additional information regarding the product [33].

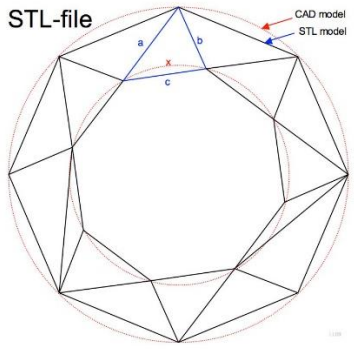

Figure 5.2 : An example of part in STL format.

5.3 CAD Model Preparation

After removing the errors, the orientation with connection to the building platform of model is decided. In the next step information related to design of part and support structure, density is assigned in a 3D model space. Based on geometry of part and orientation, the 3 D model and also support structure is sliced based on STL file into

defined quantity of layers suitable height each depicting a slice of model and supporting structure. Inside every slice the geometry is constant.

The sliced data is then transfer to additive manufacturing system for part fabrication. There is numerous software which permit these tasks to perform. For example “Magics” by Materialise is a software that integrates all CAD model procedure in one program and produce data file which is suitable for powder bed machine systems [33].

Machine step is the next step just after the software preparation in additive manufacturing process. This process consists of cleaning and removal of waste from previously build part, loading for new powder, checking all the building settings and parameters including gas pressure, oxygen sensor, flow rate etc. The next process after machine hardware setup is to execute the build data and initiate building the part, stop fabricating at any time if necessary, prepare for finished part removal, and remove material. The sequence starts from accepting and coordination of build part in vicinity of build plate. After the decision of location of part next steps are immediately executed including building process parameters, material properties, part parameter.

6. MICROSTRUCTURE AND MELT POOL

In selective laser melting process power from laser selectively melts the metal and that forms a liquid melt pool. The melt pool suddenly solidifies as the laser passes that area. The successive melting of powder by consecutive tracks forms 1 layer. These layers are together consolidated one above other to form the solid geometry according to the data od CAD model (Figure 6.1). For strong bond of tracks and adjacent layer partial remelting of previous layer and overlapping of scan track is done. This also leads to higher densification and uniform properties with required degrees of isotropy. Figure below shows the schematic view of layers and track overlapping.

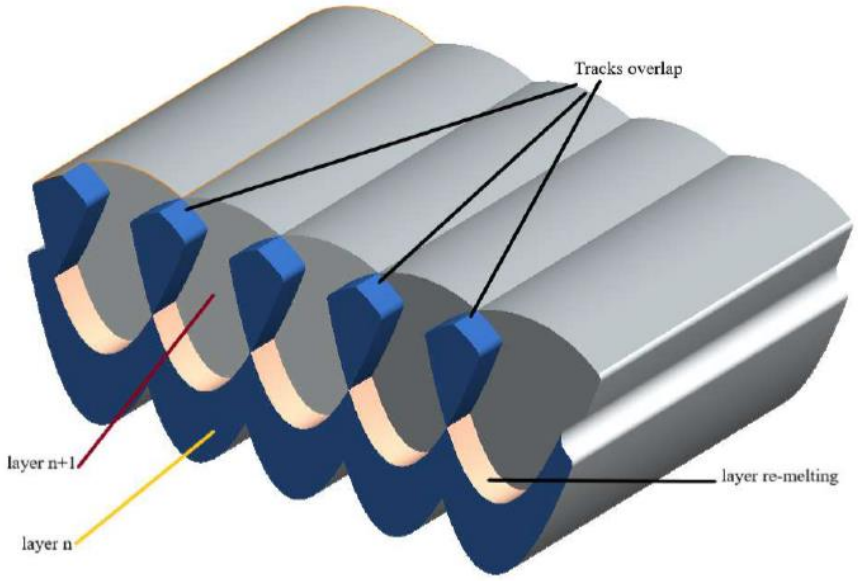

Figure 6.1 : Track remelting and layer overlapping in SLM.

6.1 Maraging Steel Microstructure

Microstructure analysis is done alone 2 directions. The first is with cross section along the build direction (cs1) whereas the other is having perpendicular to build direction(cs2). The AM built part is observed in optical microscope and scanning electron microscope. The microstructure of a part built with cs2 cross section is fabricated with travel speed of 120

mm/s and a spacing within hatch is of 60 µm and is shown on the left side of figure 6.2 below.

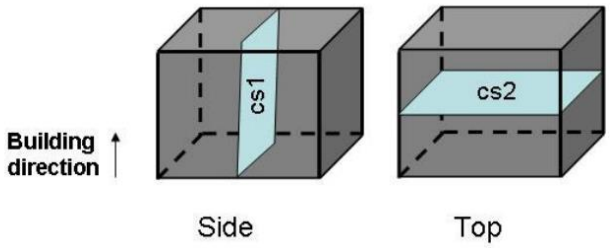

Figure 6.2 : Direction representation of scan track [31].

Bidirectional scan tracks are clearly visible. And most of the pores represented by black dots at the connection line of scan tracks. This porosity is the reason of insufficient overlap as a result of high scan spacing [34].

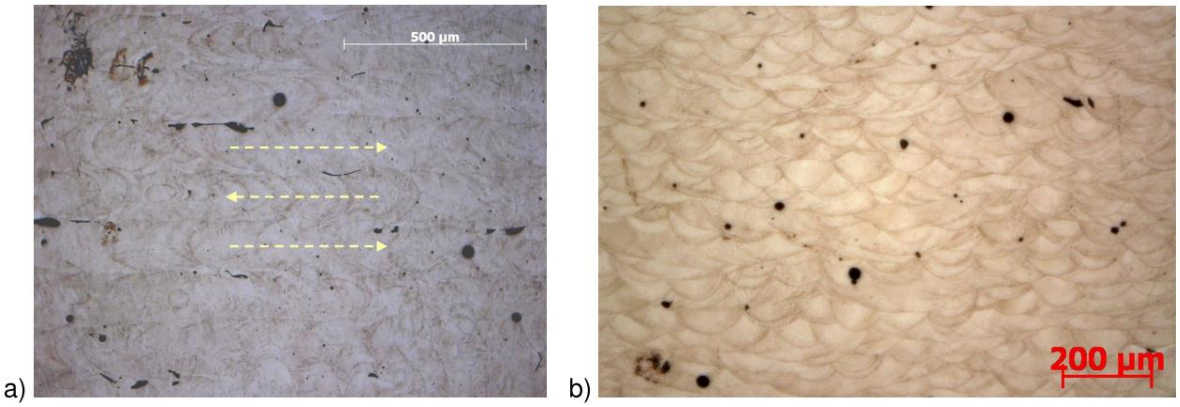

Figure 6.3 : Micrograph of etched maraging steel (a) Top/cs2 side (b) cs1 side [31].

The cs1 cross section of part built with scan speed of 150 mm/s and scan spacing of 30 µm is shown on the right of above figure. The picture shows the different melt pools formed during melting of the maraging steel. The scanning direction is perpendicular to the cross section shown. The depth of melt pool for this case is found to be 80 µm to 90 µm. The micrograph also shows that the scan vector is rotated 90 degrees in each successive layers.

The scanning electron micrograph image cs1 and cs2 side of cross section at high magnification is shown figure 6.4 below. The micrographs on the left (cs2) shows the

bidirectional scan tracks. In SLM cooling rate is fast so sudden solidification restricts formation of lath martensite.

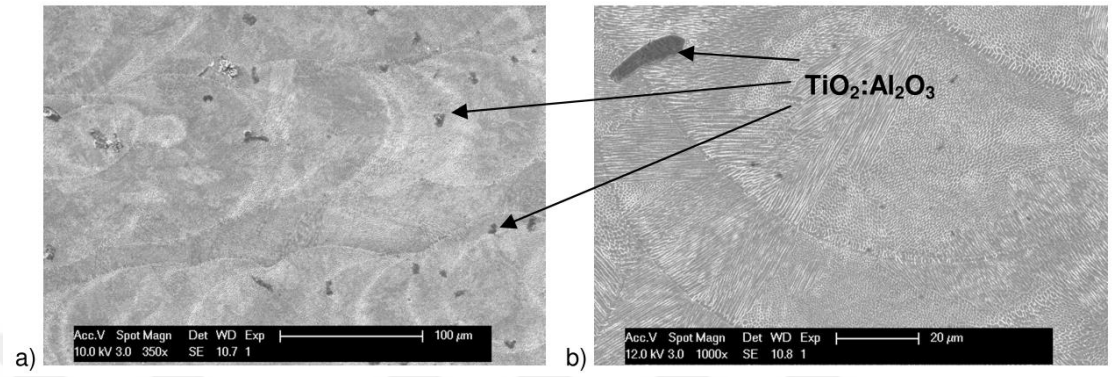

Figure 6.4 : SEM image of maraging steel (a) cs2 side (b) cs1 side[31].

The inter cellular spacing is lower than even 1 µm, which is the reason of good strength and hardness. The right side of above picture shows the dendritic morphology with epitaxial growth. Large inclusions of titanium and aluminum combined oxides (TiO_2:Al_2O_3) are present with size 10 to 20 µm as shown by dark spot in left side and elongated thick dendrite in right hand side. These are responsible for lowering the mechanical properties in aged conditions.

6.1.1 Hardening of maraging steel

As built maraging steel part is a ductile low carbon body centered cubic and has a martensitic structure. The relatively better strength and toughness of maraging steel is achieved by age hardening and aging. The aging process uniformly distribute the fine nickel rich intermetallic precipitates. These precipitates are the reason behind the strengthening of martensitic structure. And this precipitates also restricts the reversion of martensite to austenite and ferrite. It is recommended that part should not be overaged as it will lead to inversion of martensite site phase into equilibrium austenite phase, together with coarsening of microstructure. This will contribute to lowering the hardness of the part. The preferred temperature and duration for age hardening is 5 hours at 480^{o} C[31].

After heat treatment of maraging steel, traces of solidification disappear and structure is replaced by martensitic structure (Figure 6.5). The martensitic structure is coarse and appears like massive blocks, consists of bundles of parallel heavy dislocated laths. The

traces of γ-Fe(Austenite) are also found and mainly present on the martensite block boundaries.

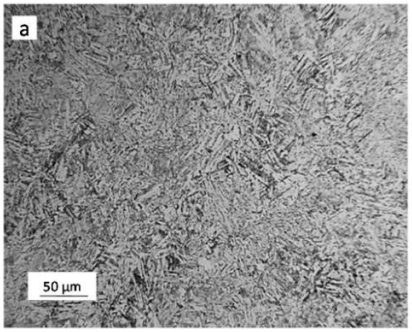

Figure 6.5 : Martensite structure after heat treatment[29].

6.2 Crystallographic Texture of AlSi10Mg

The following figure shows the crystallographic structure of melt pool of AlSi10Mg part, it can be seen that elongated grains are growing near center of the pool (Figure 6.6). Epitaxial growth occurs at some locations like center of melt. Far from the center small nucleated grains are formed.

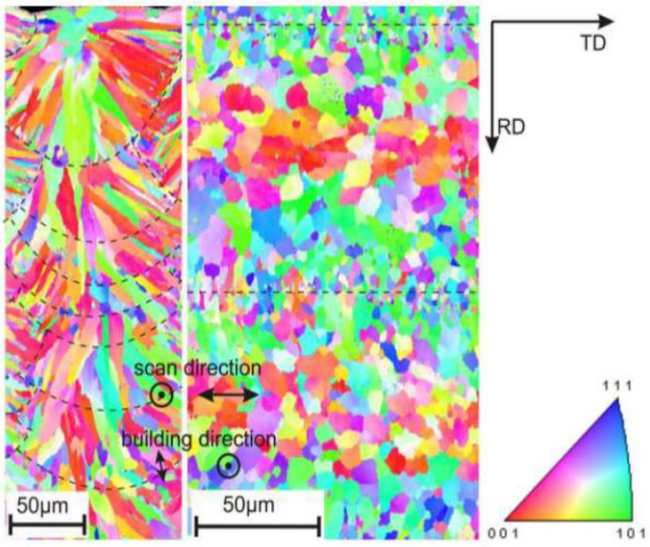

Figure 6.6 : ESDB graph of AlSi10Mg part with front view(left) and top view(right).

Few grains can grow at the center of pool. Equiaxed grains forms at top of pool. Next scanning layer remelts again the previously solidified layer which results in the

disappearance of equiaxed grains from the top of melt pool. The only grains remain are those on the top layer of last melt pool [35].

At pool boundaries tiny grains with varying colours of size less than 3 μm and random orientation are present. Larger grains with size of red color of nearly 12 μm of random orientation are present at the centerline of melt pool. Grains of nearly 6 μm are present between the border and centerline of melt pool with blue-green color[36].

In figure 4.1 small cellular dendritic structure of less than 1μm are observed. They grey area represents Aluminum covered with white fiber like Si particles. This phase can also precipitate Mg_2Si. Fine fiber like Si in aluminum results in very high Vickers hardness of nearly 127 ± 3 Hv0.5 compared to the hardness of as casted product, which is nearly 95–105 Hv.

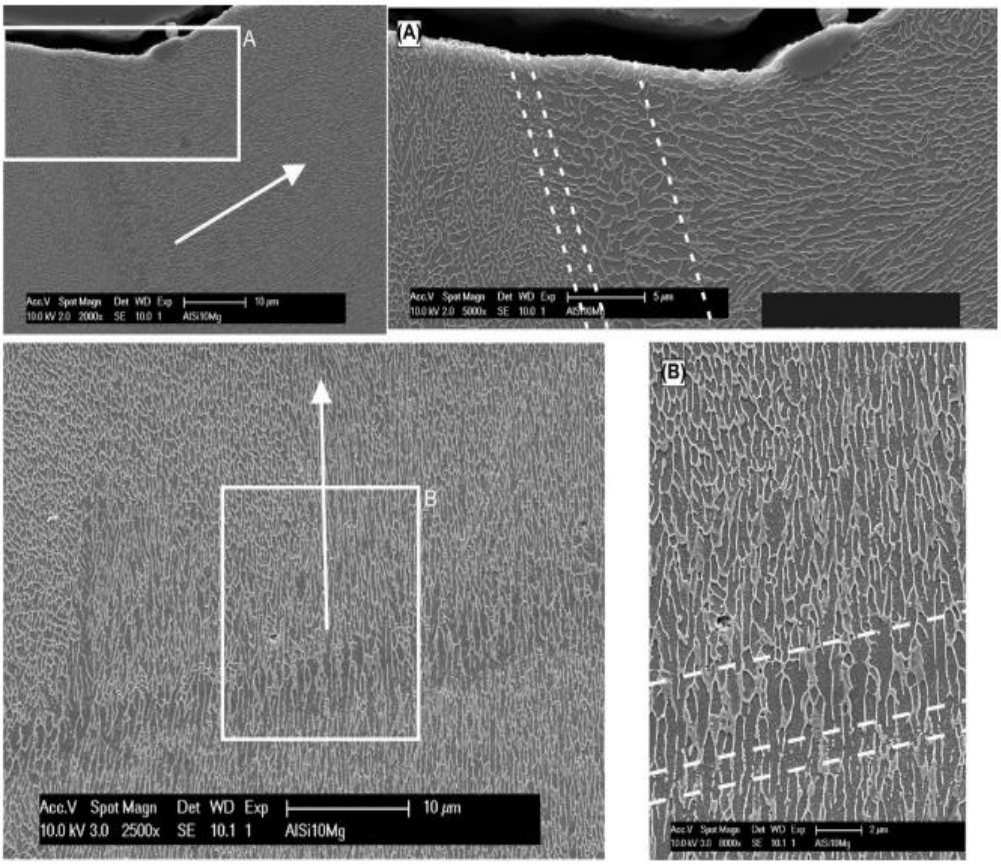

Figure 6.7 : Front and side view of microstructure of AlSi10 Mg.

There are 3 different zones across the melt pool (as can be seen in figure 23 and 24) namely fin, Coarse and Heat affected zone. Within pool the dendrites grow near center of pool. Solidification is generally cellular but sometimes extensions on sides can be observed. The size of cell is not uniform but a change from a coarser cell of nearly 0.7 μm to finer cells 0.4 μm is observed. Also structure at location A is very fine nearly 0.2 μm.

7. EFFECTS OF PARAMETERS ON ADDITIVE MANUFACTURING

There are various parameters which affects the quality of additive manufacturing, these can be surface roughness, scanning strategy, surrounding environment, power and speed etc.

7.1 Surface Roughness and Density Optimization

In this process the laser power of 170 to 210 W combined with scan speed from of 250 mm/s to 1500 mm/s is used for process optimization. At first scan speed of 105 µm is used. The density increases with increasing scan speed and reaches a maximum value. The maximum point of density varies with different scan speeds. The density vs scan speed shows a parabolic pattern. The maximum value of density reached is approximately 99.25 percent with speed ranging changes 900 mm/s to 1300 mm/s.

By fixing laser power, surface roughness reaches minimum at a specific scan speed. These speed ranges from 900 mm/s to 1400mm/s. For higher laser power, minimum lower surface roughness reaches at lower scan speed. If melt pool remains stable surface quality improves by increasing energy density.

The effect of scan speed and thickness layer of density of additive manufacturing part is be described in following paragraphs.

7.2 Effect of Scanning Strategy on Microstructure

The laser is applied with different scanning strategies. Surface roughness, porosity level, microstructure and heat buildup depends mainly on scanning strategy [1].

Samples of 15X15X15 mm^3 were produced under argon atmosphere. The parts were produced by different scanning strategies like unidirectional scanning, bidirectional scanning, rotation of scanning direction between 2 layers, dividing the scanning area into small islands called island scanning (Figure 7.1). The small islands are of cross section 5X5mm^2 and scanning direction is shifted to 1mm in x as well as y direction between

successive layers. In sample C each layer is scanned twice but rotated by 90 degrees between each scan.

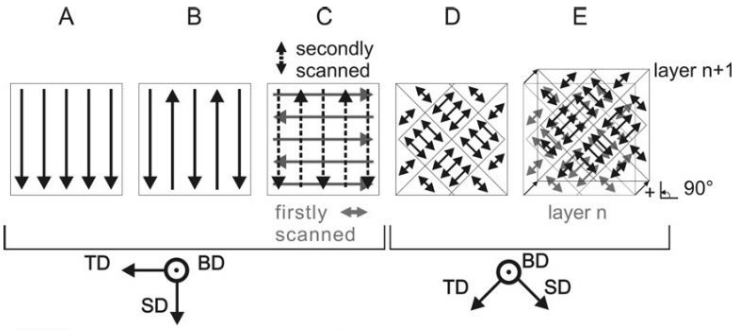

Figure 7.1 : Scanning strategies for selective laser melting.

BD, SD and TD stands for building, scanning and transverse direction.

The figure below shows that cross section view of sample A. Long scan vector can be seen on the top and side view. The cross section become visible in front view. The size of melt pool can be estimated by cross section of top melt pool in front view.

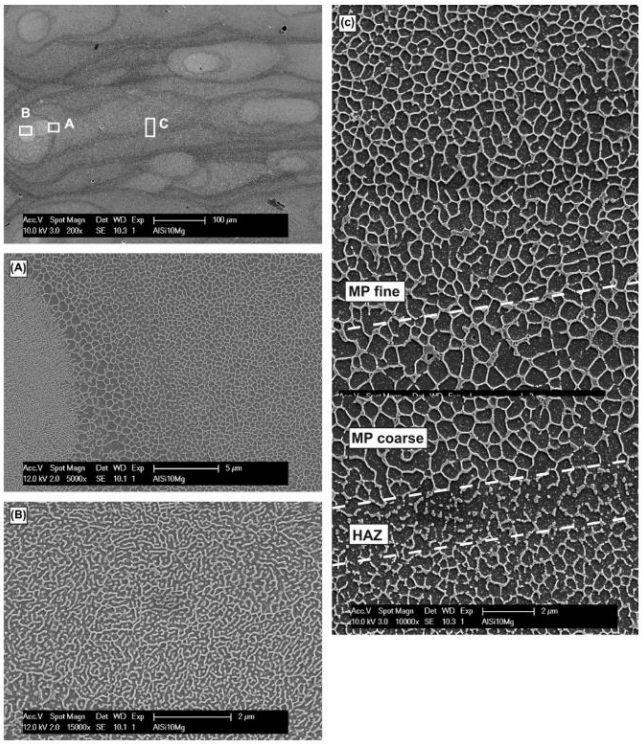

Figure 7.2 : Top view of sample B with bidirectional strategy.

It is clear that melt pool is half cylindrical. The calculated pool height is 110 ± 10 µm (of all samples), width 170 ± 15 µm (For samples A & B) and 179 ± 30 µm (samples D and E). Due to change is shape and depth of pool, they are not continuous. From figure 7.2 it can be noted that deep and steep melt pool forms at the start and ends of laser scan tracks. Heat accumulates at these locations of path and keyhole pool forms [37].

7.3 Effect of Oxygen

Oxygen reacts with molten metal at high temperature and forms metal oxide. The metal oxide is mainly found at the edges because of the continuous melting at top and bottom. Most of the metal oxides in additive manufacturing are found in aluminum as they are hard to break. The reason behind this phenomenon is high melting point of aluminum oxide which reaches even 2000 ^{o}C whereas the melting point of aluminum is just 660 ^{O}C.

At high temperature the aluminum reacts with oxygen and forms aluminum oxide. This aluminum oxide is hard to detect as it is hidden inside the melt pool (Figure 7.3). In order to avoid the trapping of oxygen and oxide formation, it is recommended to use high incident heat which will melt the oxide film on the previous layer.

Better scanning strategies and scanning parameter, use of noble gases like argon can significantly control the formation of oxide. However, the complete removal of oxygen is very difficult as 0.1 to 0.2% oxygen is always present in environment. Figure below shows the oxygen trapped after the part is fractured [26].

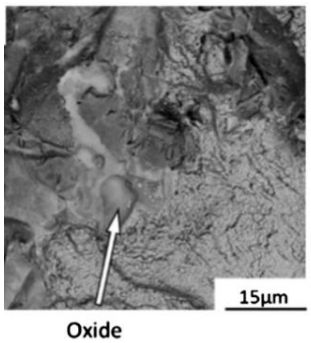

Figure 7.3 : Oxygen trapped in SLM part.

7.4 Effect of Power and Scan Speed

In this case a laser power between 165 W and 205 W is combined with speed of 210 mm/s to 1500 mm/s. Top view of scan tracks built with different combination of parameters is taken for comparison study. The speed range of < 600-700 mm/s results in irregularities and distortion because of balling phenomena. By increasing the energy P/v, pool volume become bigger and viscosity reduces. While decreasing P/v, recoil pressure become significant and distort scan tracks. By further increasing the scan speed energy given is not enough to melt powder and some proportion of melt the substrate. Which results in instability and formation of droplets[16] [2].

The red hatched area represents the more favorable parameters for AM parts (Figure 7.4). The parameters that are chosen outside shaded area will result in unstable scan tracks. Low energy of 170 W combined with speed of 1400 mm/s causes droplet formation and very bad wetting. While high energy (P=205W and speed = 210mm/s) results in deep penetration and some evaporation of particles of powder.

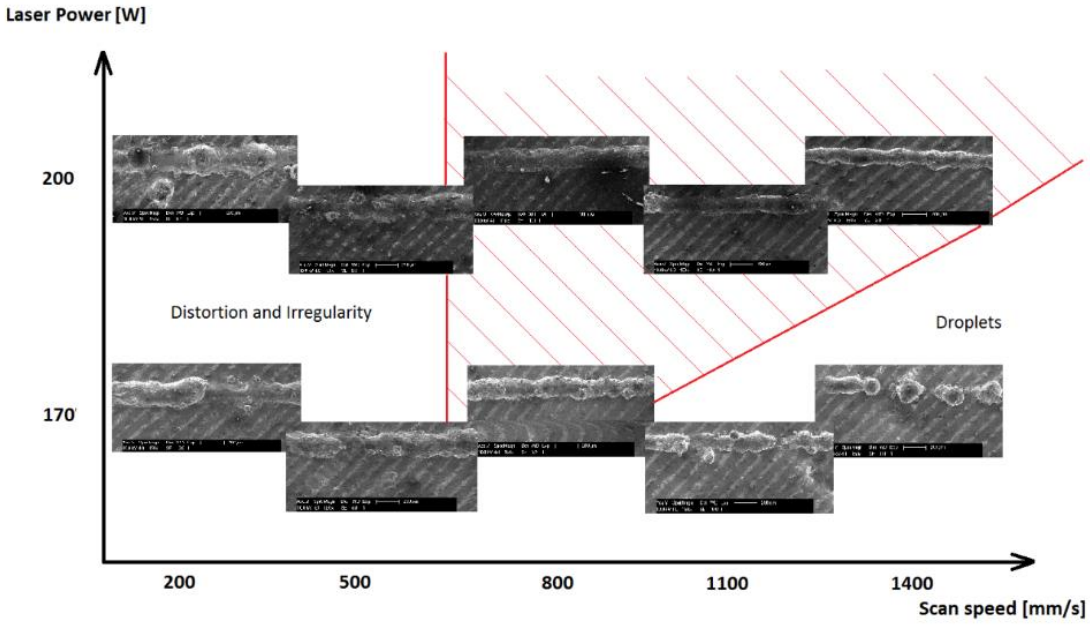

Figure 7.4 : Laser speed vs power optimization.

7.5 Effect of Relative Density

The chart below depicts, impact of scan speed at relative density of additive manufacturing maraging steel. The maximum possible density data received till now is 99% of theoretical density on Concept Laser M3 equipped with Nd:YAG laser. These values are obtained by altering the thickness 30 µm to 60 µm. It can be noted that the relative density decreases with increasing scan speed. The reason of this decrease in density is the reduction of energy supplied per unit area by laser. Although this reduction is not significant at lower scan speed. The results show that due to varying layer height from 30 µm to 40 µm results in 25 % reduction in scanning time while very little reduction in density (Figure 7.5). By much lowering scan speed, reduction in density is obtained due to balling effect[29].

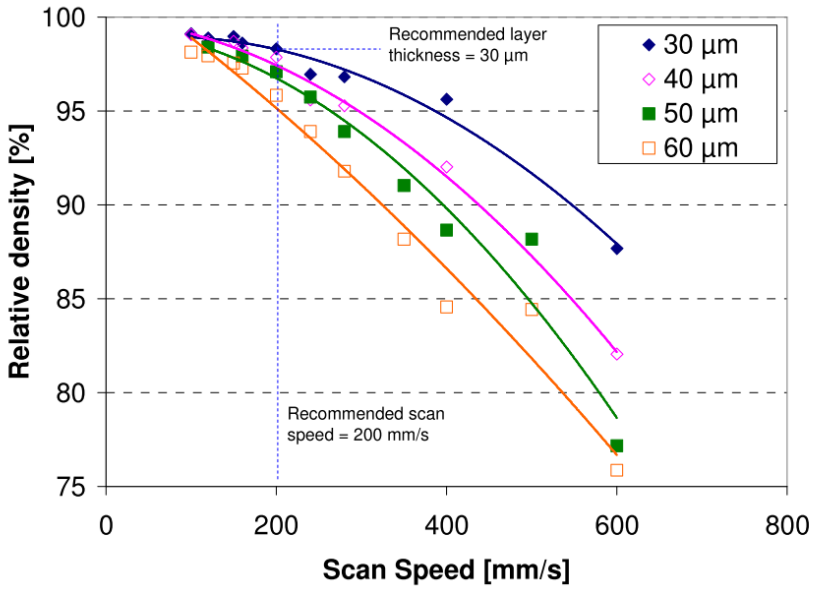

Figure 7.5 : Effect of scan speed on density [38].

7.6 Effect on Surface Quality

The samples are produced with different scan speed and different thickness, then the surface roughness R_a is taken on top surfaces of each test. It is concluded that the variation of surface roughness is not significant with speed for lower thickness values of layer that is 30 µm and 40 µm. While for high thickness of 60 µm, the surface roughness value decreases by varying laser travel speed from 200 mm/s to 600 mm/s (Figure 7.6) [39].

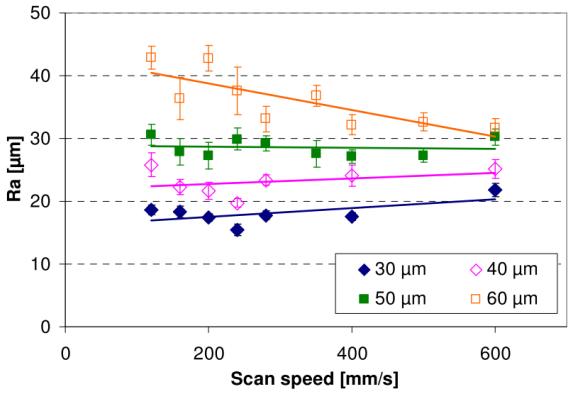

Figure 7.6 : Effect of scan speed on surface roughness[31].

7.7 Effect on Hardness

Micro and macro hardness tests are conducted on specimens with different with different scan speed and layer thickness. In order to analyze the effect of porosity on different hardness, Rockwell hardness test is conducted for macros analysis. The hardness depends on density. The following figure 7.6 shows that for lower speeds of nearly 200 mm/s, there is very little change of hardness with scan speed as well as layer thickness as the densities are not significantly dependent on the parameters in this region. But for higher speed the hardness has reduced because of increase in porosity.

For micro hardness test conducted by Vickers hardness test, it is found that at low speeds the hardness is not significantly dependent on speed change and layer thickness [40].

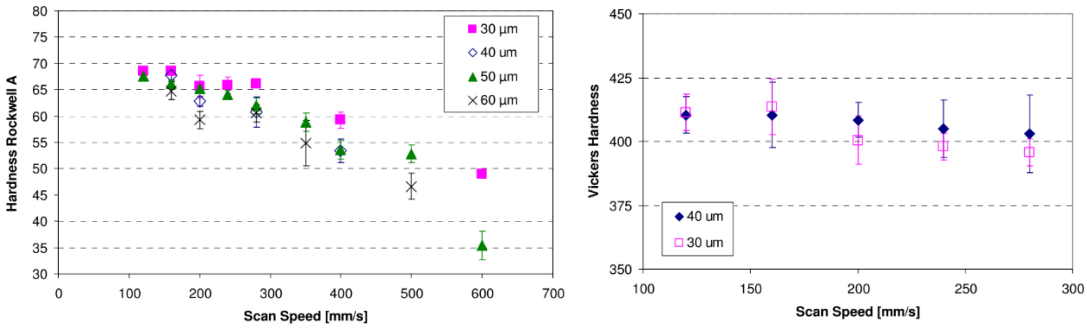

Figure 7.7 : Rockwell and Vickers hardness test of specimens [31].

8. DEFECTS IN ADDITIVE MANUFACTURED PARTS

There can be various kinds of defects including fracture, porosity, surface roughness, crack and delamination etc.

8.1 Fracture

From the fractured surface (Figure 8.1) of additive manufacturing part, it can be interpreted that the fracture is ductile type, consisting of 3 steps. Namely void nucleation, their growth and then coalescence. Large voids forms from preexisting defects like unmelted powder particles, splats. Cavities originates from incomplete melting between successive layers. Right side of the following figure shows the nucleation site, here the development of crack mostly occurs by quasi-cleavage decohesion mechanism [41].

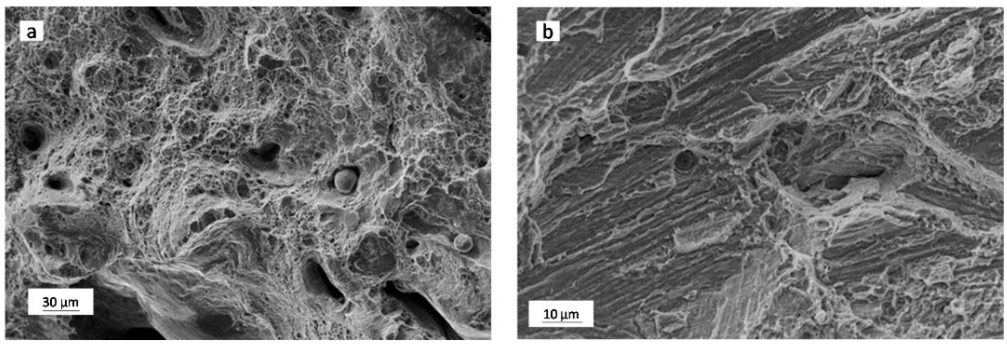

Figure 8.1 : Broken tensile surface (a) as built sample (b) sample aged at 460^{o} C[29].

8.2 Porosity and Lack of Fusion

Porosity and lack of fusion defects are very famous in additive manufacturing. They negatively influence the properties of fabricated part and hence need to be eliminated or minimized. There are mainly three mechanisms responsible for these type of defects. First type of defects occurs when very high power intensity is used or keyhole mode is used. If care is not being taken in keyhole mode, it becomes unstable and forms and collapse several times, resulting in entrapment of porosity of nearly spherical shape. Figure 8.2 (a) below shows keyhole porosity in 316L stainless steel manufactured via additive

manufacturing. Secondly a gas is trapped in powder when atomization of powder or a shielding gas during manufacturing [15]. These microscopic porosity is also spherical in morphology as shown in figure 8.2 (b) below.

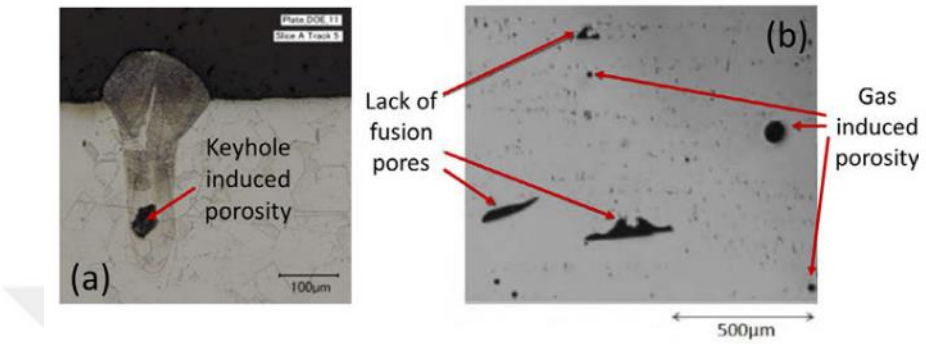

Figure 8.2 : (a) Keyhole porosity (b) lack of fusion and gas entrapment porosity.

Improper fusion of molten pool into previously deposited layer causes lack of fusion porosity. Improper penetration leads to the formation of defects that are elongated in shape and having a larger dimension of nearly 10 µm[42]. By increasing the scanning speed melt pool size decreases, penetration in successive layer reduces leading to high susceptibility to lack of fusion porosity as shown in figure (a) below. However, by increasing the power of laser, the penetration depth can be increasing by increasing melt pool size leading to higher penetration shown by figure (b).

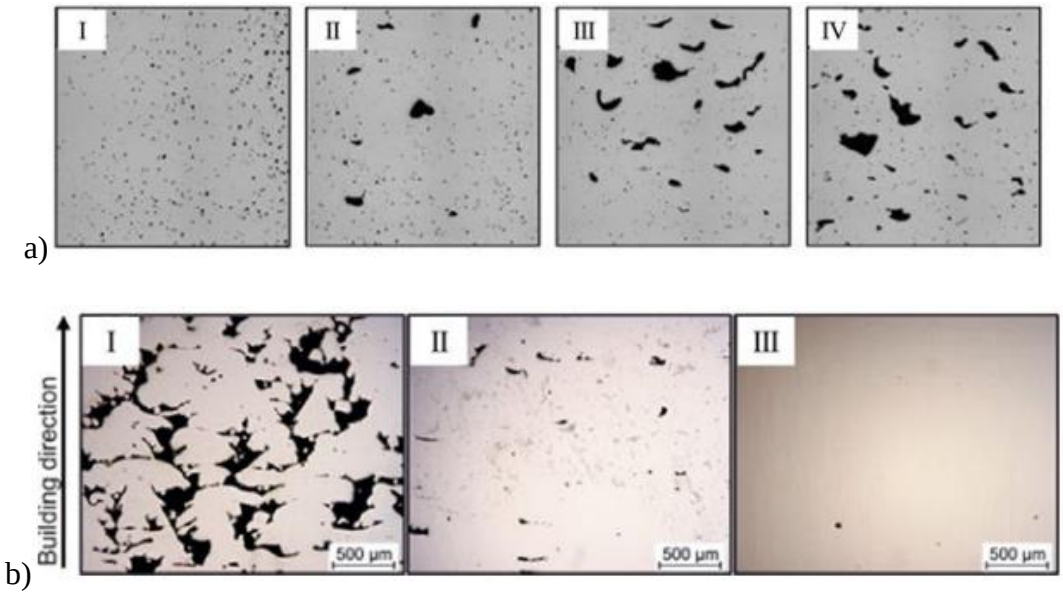

Figure 8. 3: (a) Effect of speed on porosity (b) effect of power on porosity.

8.3 Surface Roughness

The surface roughness of part is dependent on several independent variables like, part design, material, process parameter, process type, finishing and post processing. Material properties includes, particle side distribution. Part design and process type includes part orientation, geometry and support structure. Process parameters include scan speed, laser power, overhanging geometry, path profile, scanning strategy. Post processing steps includes part removal, chemical treatment, polishing, machining etc. [14].

Surface roughness can be caused by “stair step effect”. Greater the layer thickness, greater is this roughness. This roughness can be reduced by tradeoff between layer thickness and time to manufacture a part [43].

The other reason of surface roughness is improper melting of powder particle. This may be a result of insufficient laser power or higher scanning speed; hence the powder particles stick at the surface of product. Higher scan speed may result in the elongation of melt pool. Due to this process the melt pool broke into small islands leading to balling phenomena as shown in figure below [44].

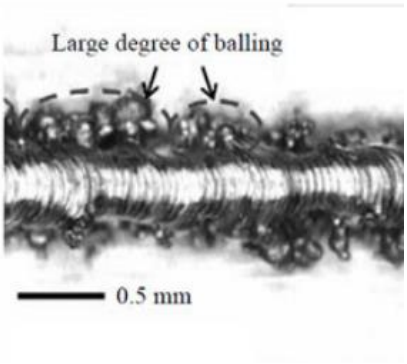

Figure 8.4 : Balling phenomena.

Low scanning speed and higher heat input can result in complete removal of balling process. Larger powder particles are difficult to melt, so a part fabricated with larger powder particles can exhibit poor surface finish.

8.4 Delamination and Cracking

Cracking is seen at grain boundary (Figure 8.5). Solidifying layer tries to reduce its volume due to shrinkage as well as contraction due to reduction in temperature. While this contraction is prevented due to adherence of previously solidified layer to new layer. In doing so tensile stresses are developed into the upper layer. If these tensile stresses are greater than the strength of metal, it leads to the formation of crack.

Liquation cracking is common in mushy zone (Figure 8.5). In partially melted zone, rapid heating causes melting of low temperature substance such as carbide. During solidification those partially melted zone suffers tensile forces as a result of thermal contraction and solidification shrinkage. There is a large difference in solidus and liquids temperature in alloys like nickel based alloys, high solidification shrinkage because of large size melt pool as in Ti-6Al-4V. Cracking may be very long reaching several layers or may be small consisting of only single layer. The figure below shows the difference.

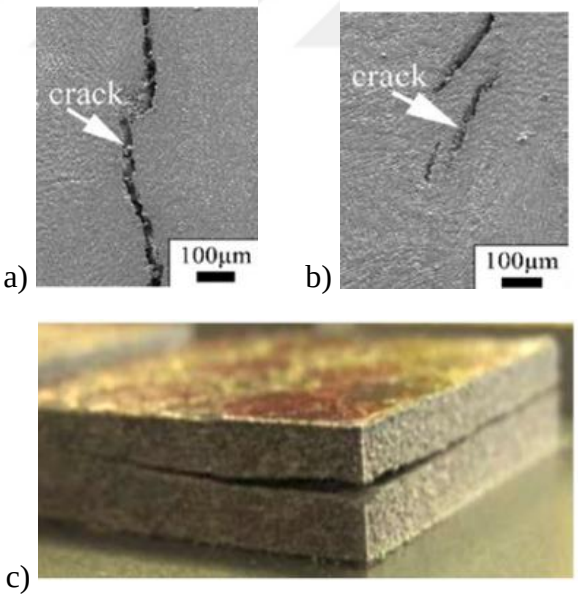

Figure 8.5 : Cracking (a & b) and delamination (c) in additive manufacturing.

The delamination arises from the separation of layers or residual stresses at the connection of 2 layers. Moving laser source causes the localized heating and cooling of material due to travelling heat. Thermal contraction and expansion due to cooling and heating. Uneven distribution of elastic strain.

9. MELT POOL MODELING OF MARAGING STEEL

The main purpose of this thesis is the modeling of melt pool, estimation of temperature profile, maximum temperature and melt pool depth in maraging steel additive manufacturing components. Study and simulation is done using APDL part of ANSYS analysis software (Figure 9.1).

ANSYS is used for the finite element analysis of the component in order to simulate the temperature distribution, structural analysis, electromagnetic analysis etc. This software is used to simulate the working conditions in virtual environment. Before starting the analysis material properties such as elastic modulus, young modulus, density, initial temperature, thermal conductivity, specific heat, coefficient of thermal expansion etc. are entered into the software either using user interface or ANSYS codes. In the next step, the material model is either exported from the CAD geometry or it can be designed in ANSYS itself. Followed by main step where boundary conditions including loads, heat flux, temperature, current, voltages etc. are defined.

On the basis of input data, the problem is being solved and further post processing is done in order to view the results, plot the necessary graphs.

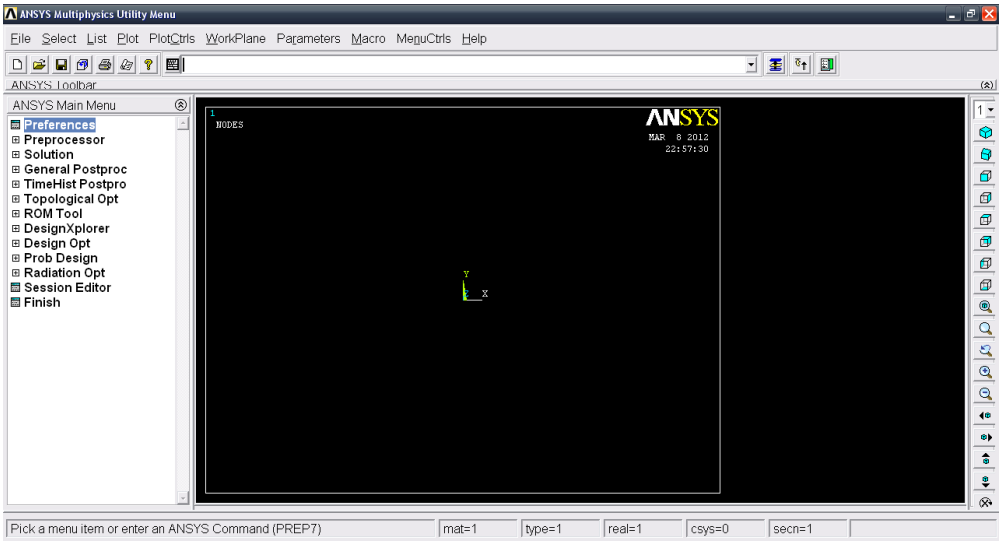

Figure 9.1 : ANSYS APDL software user interface.

The above figure shows an image of ANSYS APDL user interface. However, the analysis can also be executed by entering the program in the top of the column given. The options on the left side are given to enter the mechanical properties, boundary conditions, view the results etc.

The performing a specific type of analysis, different types of elements are used. These elements have inbuilt equations for solving problems related to different types of environment. This element type also effects the accuracy of result and time consumption in simulation. For the same environment and boundary conditions different element types can be chosen. In the present study two element types PLANE55 and SOLID70 are chosen. PLANE55 (Figure 9.2) is designed for steady state or transient thermal analysis and having single degree of freedom temperature at each node. Similarly, the same conditions apply to SOLID70 (Figure 9.2) except that it is used for 3D analysis.

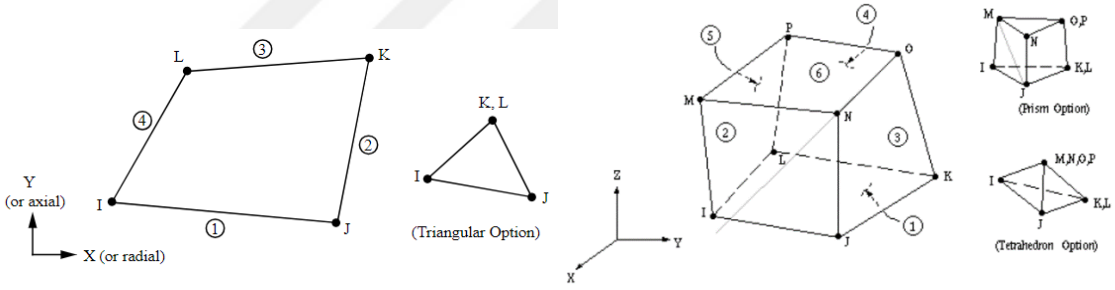

Figure 9.2 : Element built structure of PLANE55 and SOLID70.

9.1 Modeling and Meshing of Structure

For performing an analysis in ANSYS it is necessary to divide the part into small meshes. The main purpose of meshing is to perform efficient, accurate and micro analysis. Whole load which is being applied on body is distributed in each mesh and analysis is done in every mesh. Convergence, accuracy and speed is dependent on meshing. The better the mesh, the accurate the solution. There are various methods of generating mesh. It can be tetrahedral, hexahedral, surface meshing, multizone method. Accuracy of results and timing for simulation varies with the type of meshing.

The basic step of any process starts with building a model. In present analysis a small cuboidal shape model is chosen to do the analysis. Model is having the dimensions of x = -0.4e-3 m, y = 1.5e-3 m, z = -0.35e-3 m. The figure 9.3 below shows the model built in ANSYS APDL.

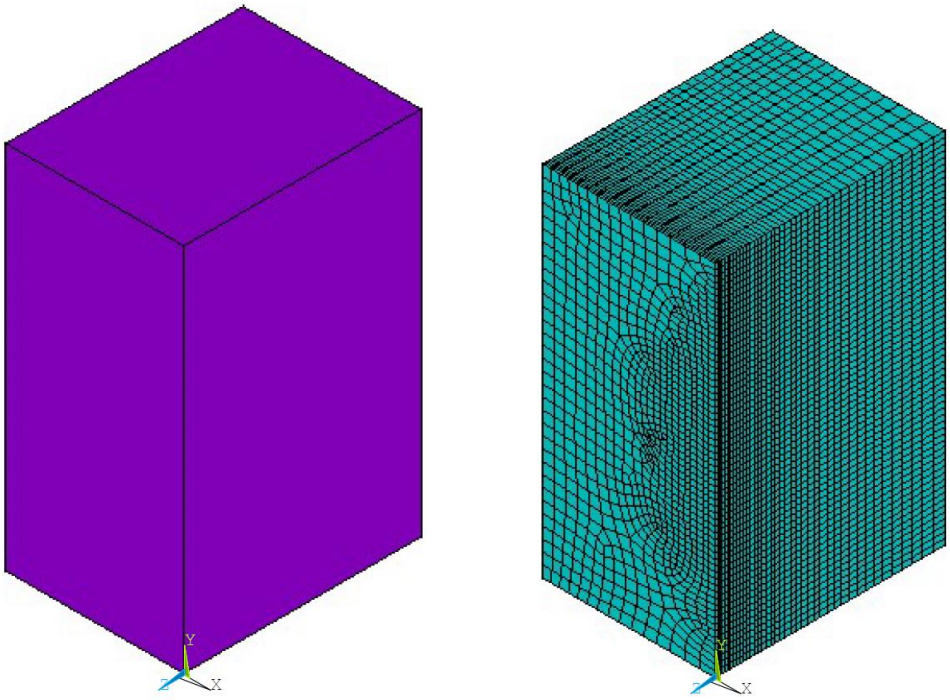

Figure 9.3 : ANSYS modeling and meshing.

Y direction in the above figure shows the laser scanning direction, while z direction is the built direction. Layers upon layers are added one above another in the Y direction in order to fabricate the whole geometry. The above geometry shows the solid model which is including solid metal geometry and above which lies a powder.

The laser melts the powder and after melting that track is added to the base. More and more parallel tracks are added to form 1 layer. The process continues and layers combine together to form a whole geometry. The powder and solid metal base is shown clearly in the figure below. The powder is filled around and above the solid geometry. While the laser is selectively melting the power to melt and form solid geometry. The remaining part still remains powder.

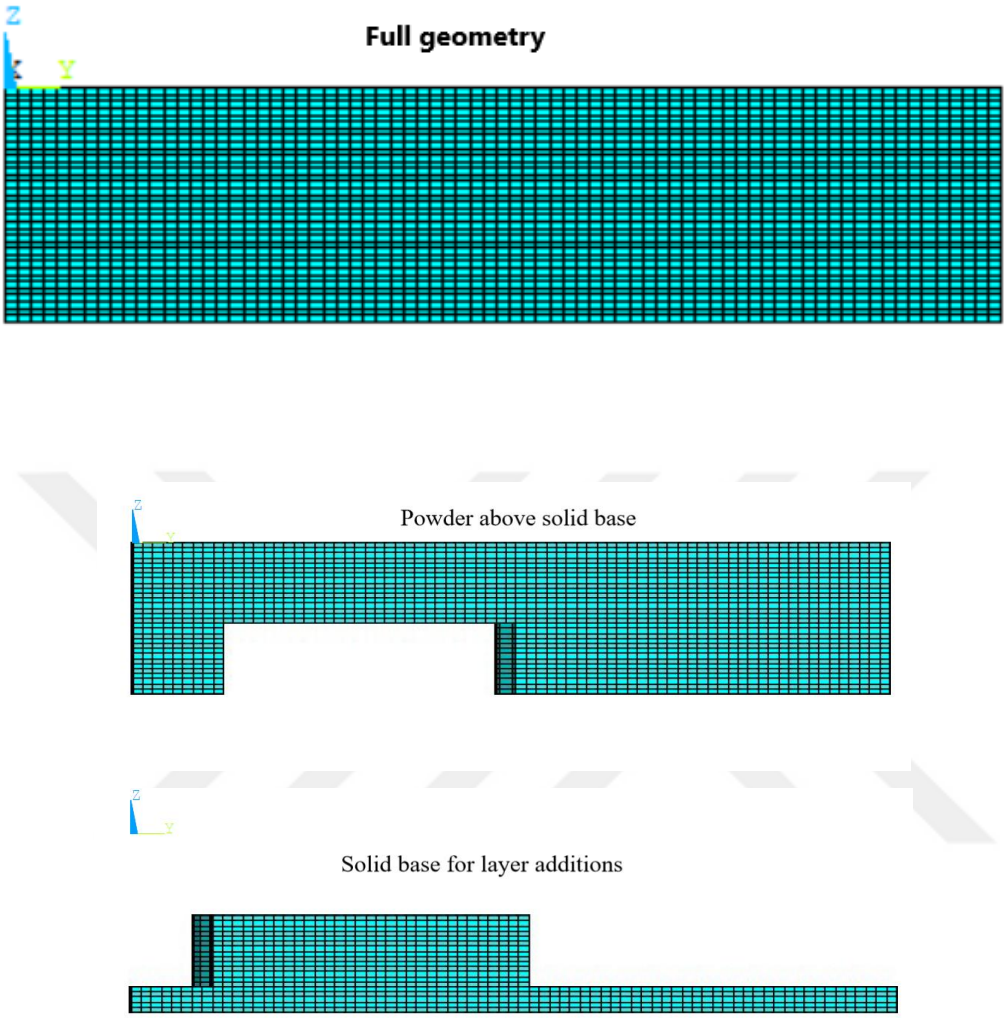

Figure 9.4 : Solid base and powder above solid geometry.

In present analysis, multizone method is used. As it divides the geometry into small cubes. Finer mesh takes more time for analysis. To avoid time consumption, coarse mesh is used on part of body with little interest while finer mesh is done on the area of interest. The maximum number of nodes formed are 39401 and elements are 36818.

9.2 Paremeters in Analysis

The basic parameters (figure 9.4) for quantifying additive manufacturing are laser power P_L, scan speed V_L, Distance between laser scan tracks Δ_{XY} and layer thickness h. The

energy of laser beam on powder bed and relation between these parameters is clarified by following equation.

$$E_L = \frac{P_L}{V_L} \tag{9.1}$$

$$E_v = PL/(V_L^* \Delta_{XY}^* h) \tag{9.2}$$

Where, E_L is the energy per unit length and E_V is energy input per unit volume.

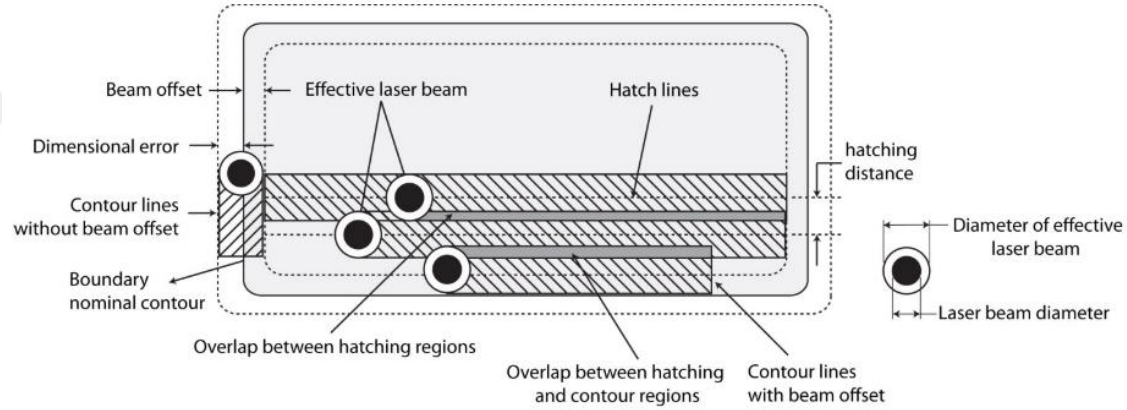

Figure 9.5 : Parameters used in the analysis.

In this case the power input is taken as 80W, 100W, 120W in combination with speed of 400mm/s, 600mm/s, 800mm/s and 1000mm/s. The thickness of each layer is 40 µm and laser scan speed as 1000 mm/s. When laser is incident upon the powder layer it penetrates till certain depth into the powder as well as previously formed layer. The effect of this penetration leads to the remelting of previously formed layer of powder which results in met pool depth of approximately 3 layers thick. So in this study penetration depth is assumed as 100 µm. The diameter of incident laser or spot diameter is taken as 100 µm. The element birth and death technique is used in performing the analysis.

9.3 Results of Analysis in ANSYS

The analysis of additive manufacturing is done in ANSYS using the properties of maraging steel material. Some of the properties of maraging steel materials are given in table 4[45]

Table 9.1 : Properties of maraging steel solid and powder.

Property	value
Thermal conductivity (Solid)	25 W/mk
Thermal conductivity (Powder)	0.1 W/mk
Density of solid material	8 g/cm^3
Density of powder material	4 g/cm^3
Specific Heat Cp	0.5 J/g/^{o}C
Melting Temperature	1413 ^{o}C

These properties are at fixed temperature and don't change with temperature. While during analysis temperature dependent properties are taken into account. The melt pool shape, size and temperature distribution is shown in the following figure 9.5 to figure 9.8

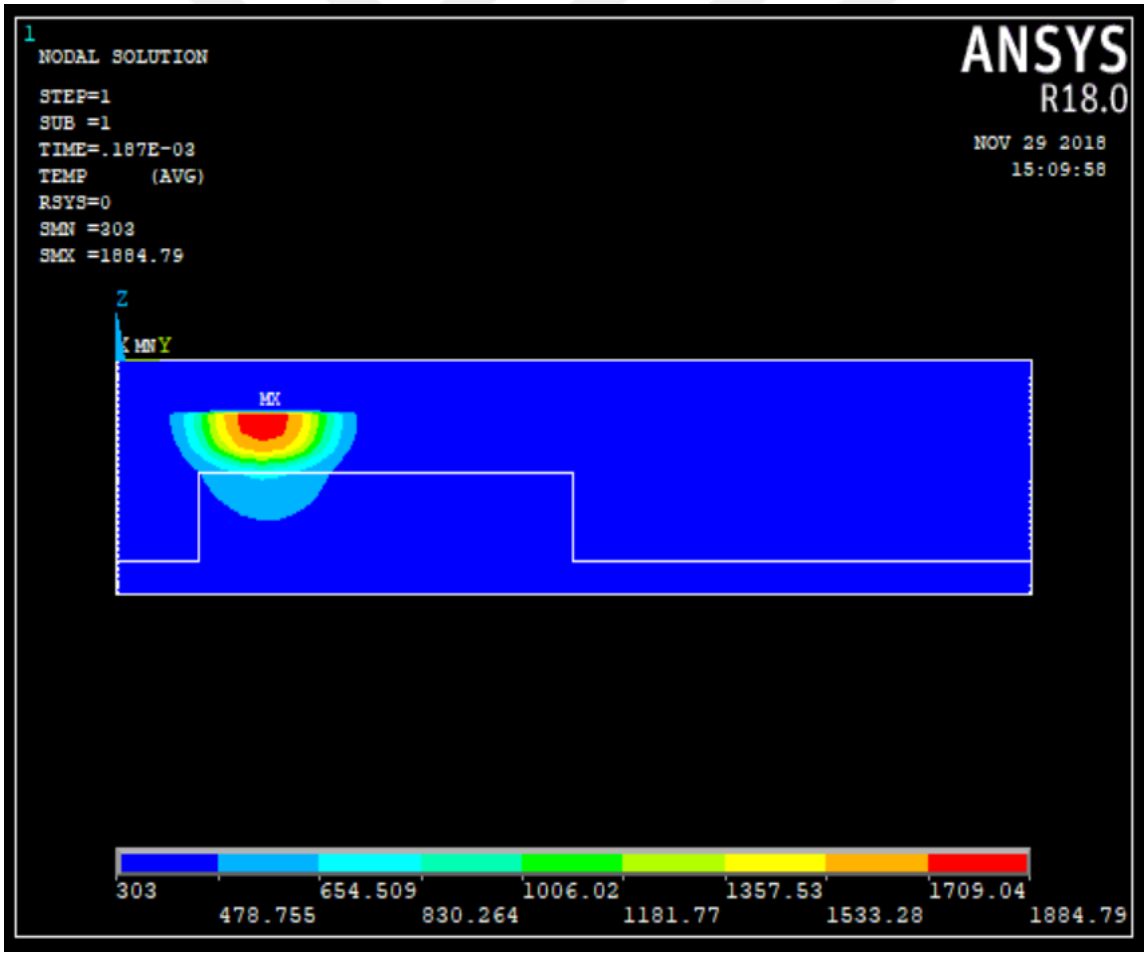

Figure 9.6 : Melt pool at 1st incident laser.

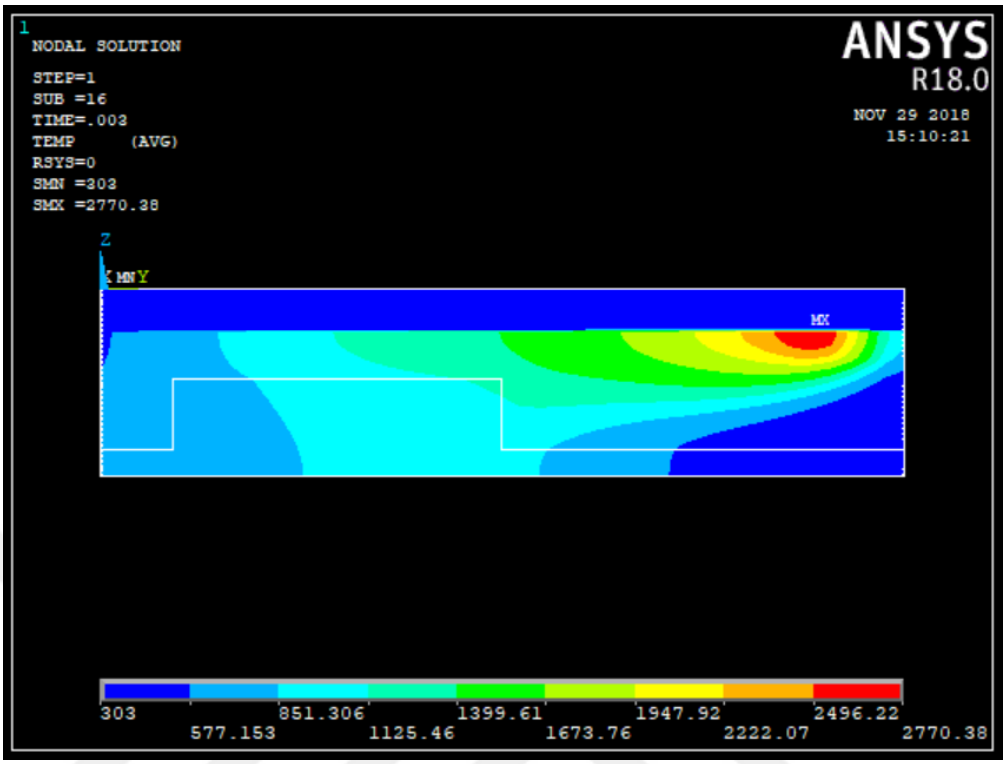

Figure 9.7 : Melt pool shape at the end of scanning of first layer.

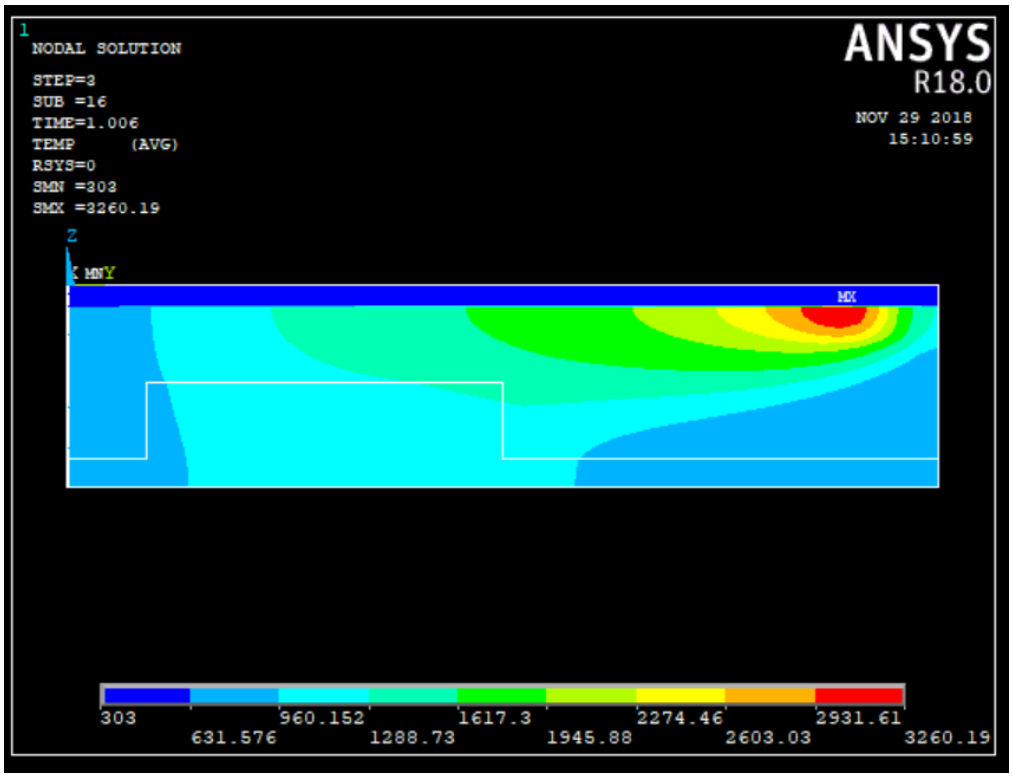

Figure 9.8 : Melt pool shape at the end of scanning of second layer.

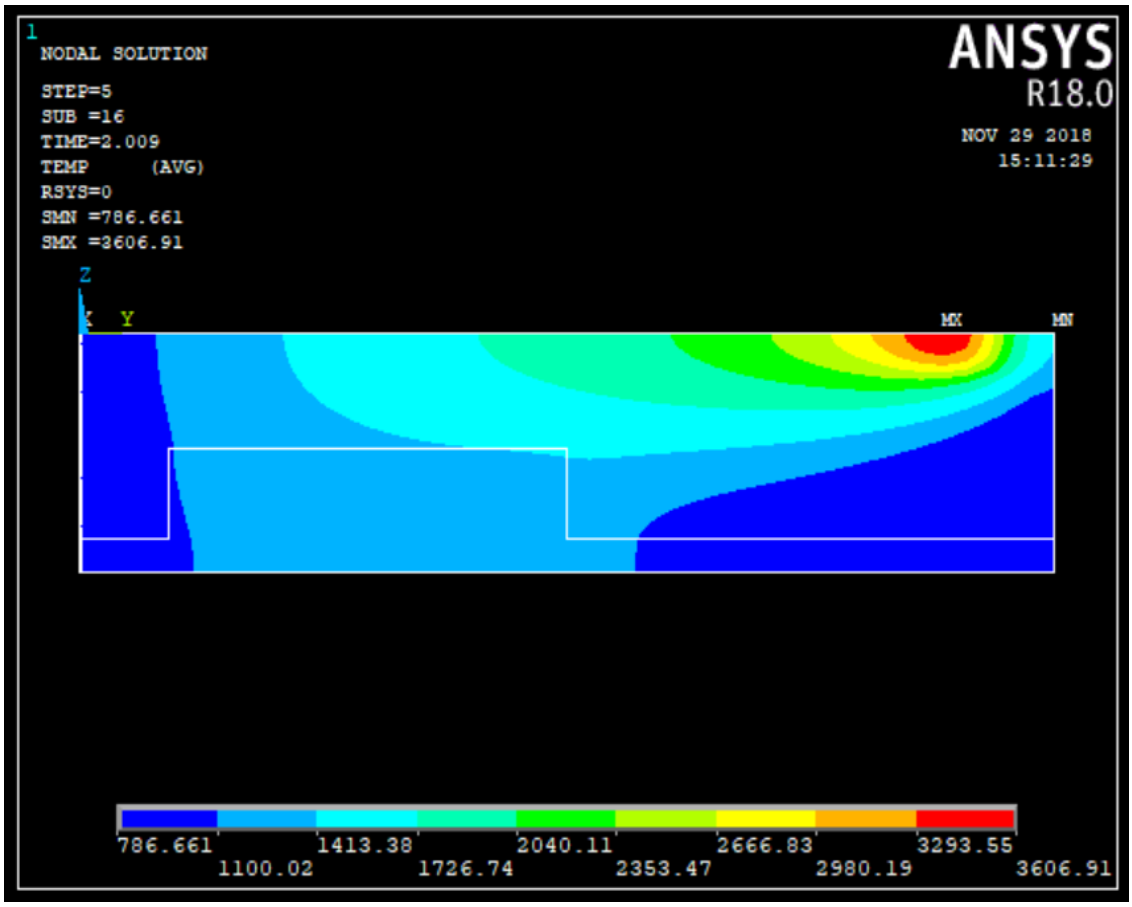

Figure 9.9: Melt pool shape at the end of scanning of third layer

Analysis is done using 3 layers of maraging steel as including more layers will increase the simulation time. The melt pool shape is predicted at the end of laser scanning of each layer. It can be interpreted that the melt pool at the starting of incident laser is very small in size. As the laser proceeds, the temperature increases as well as the size of melt pool increases. The reason behind this phenomenon is that as time passes more and more heat starts dissipating into the surrounding powder.

Based on the combination of parameters many different outcomes are evaluated. These include temperature and melt pool depth. These are the most important and basic factors that defines the performance in additive manufacturing. Temperature decides the size of grain formation after cooling. Melt pool depth is the primary variable for checking the adequate fusion of layers upon layers. The following table lists the temperature and melt pool depth for different combination of parameters.

Table 9.2 : Result of temperature and melt pool at different combination of power and speed.

S. No	Power W	Speed mm/s	Temperature (K)			Melt pool depth (µm)		
			Layer 1	Layer 2	Layer 3	Layer 1	Layer 2	Layer 3
1	80	400	2200	2479	2710	60	75	85
2	80	600	1923	2135	2287	45	55	65
3	80	800	1762	1922	2030	25	45	55
4	80	1000	1666	1790	1876	0	30	45
5	100	400	2477	2865	3163	70	85	105
6	100	600	2138	2410	2587	55	65	75
7	100	800	1935	2135	2292	45	55	65
8	100	1000	1805	1958	2067	30	45	55
9	120	400	2770	3260	3606	80	95	115
10	120	600	2367	2674	2925	60	75	85
11	120	800	2100	2366	2536	55	65	70
12	120	1000	1943	2134	2296	45	55	60

The values of temperature and melt pool depth which are listed in above table are drawn into the following graph for better understanding of their variation with change of power and speed.

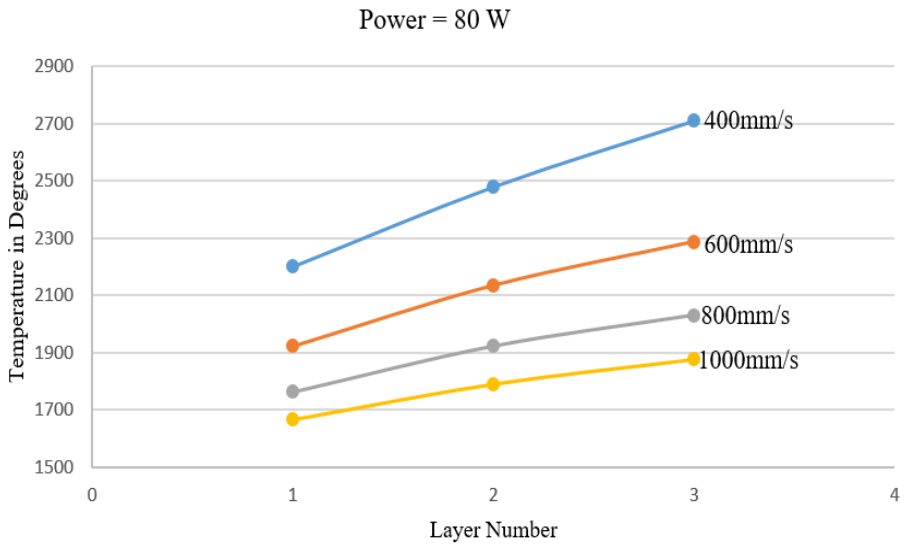

Figure 9.10 : Temperature variation of layers with 80 W power and different speed.

It can be inferred from table 9.2 that the value of temperature as well as melt pool depth increases with each layer as well as their values increases with lowering speed.

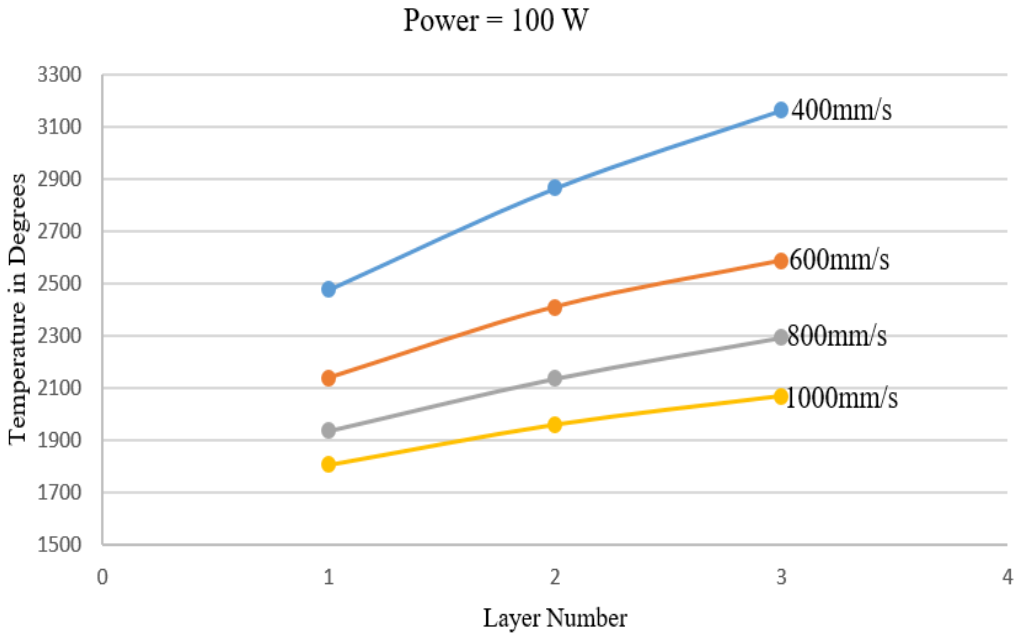

Figure 9.11 : Temperature variation of layers with 100 W power and different speed.

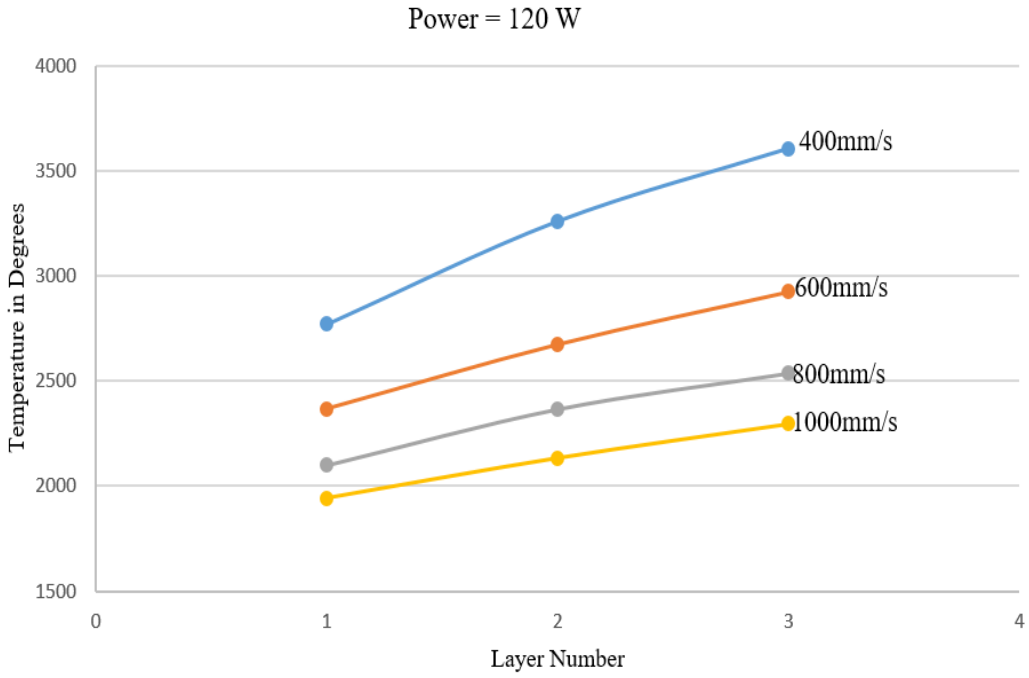

Figure 9.12 : Temperature variation of layers with 120 W power and different speed.

It can be inferred from the chart that the temperature rise with layers follows almost linear trend. During the first layer, the maximum temperature reached into the melt pool is more than 1st and 2nd layers. The first layer is totally surrounded by powder and the thermal conductivity of powder is very low. In case of maraging steel the powder have a thermal conductivity of 0.1 W/mk. So very minimum amount of heat energy is dissipated into the surrounding powder in the first layer. But during the deposition of second and third layer the maximum temperature increases linearly. In case of 2nd and 3rd layers, the powder layer is added on previously melt layer of metal. So the heat from laser in addition to heat from previously warm layer causes temperature to rise further. But as more and more layers are added, this difference in temperature between consecutive layers decreases and at the end temperature of every layer becomes constant as process proceeds.

As the speed is reducing or power is increased so the total energy per unit volume increases, which results in rise of temperature.

The following graph depicts the variation of melt pool depth for combination of power and speed as well as its variation with further layer addition.

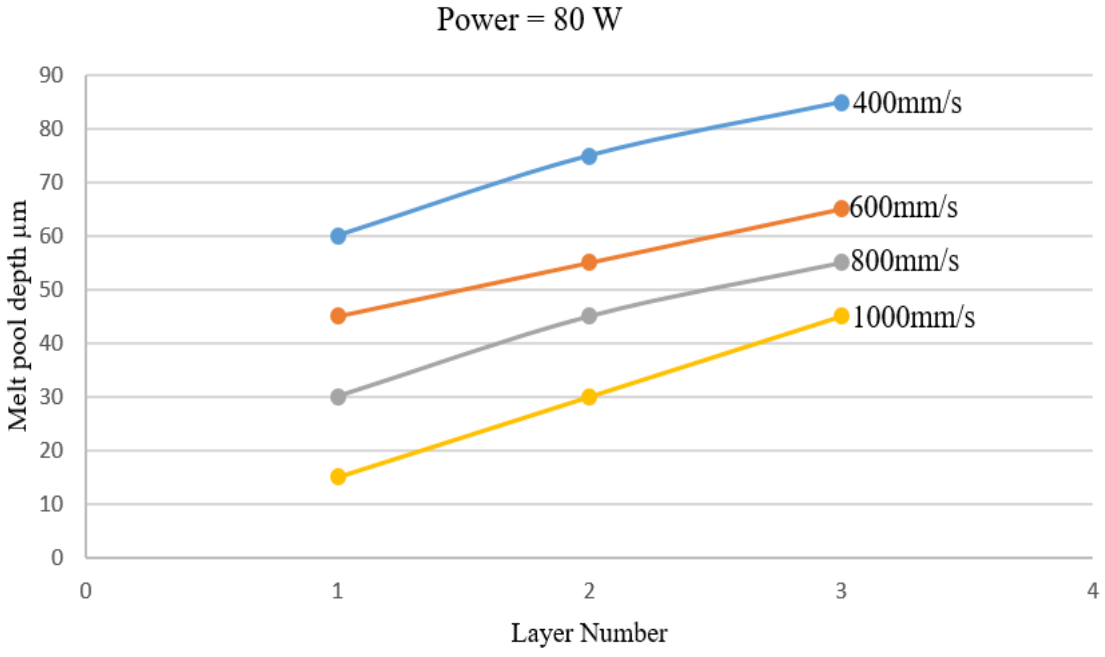

Figure 9.13: Variation in melt pool depth for 80 W power and combination of speed

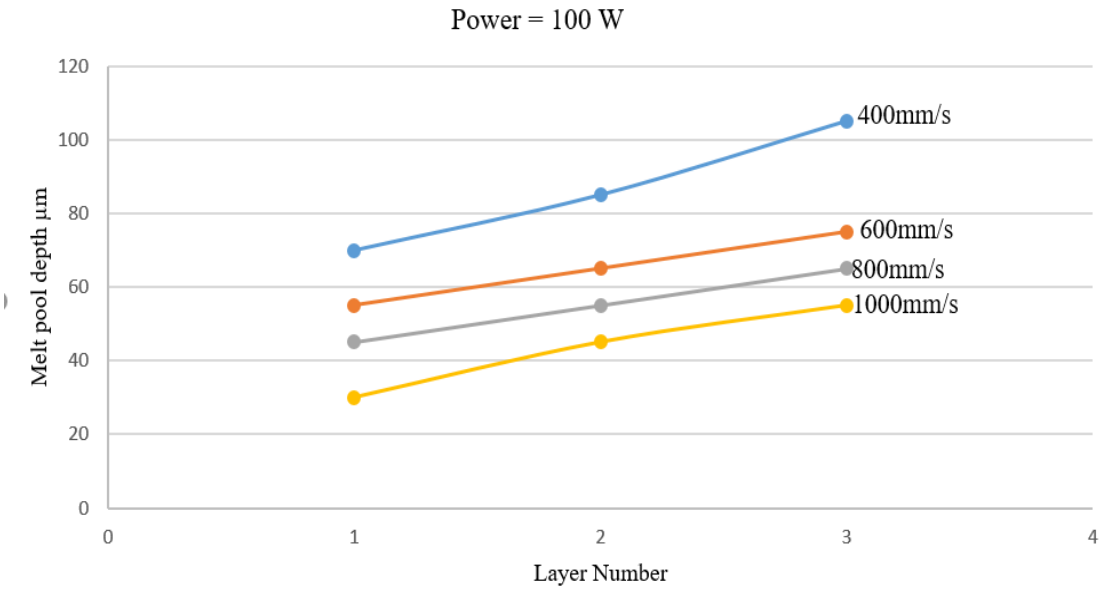

Figure 9.14: Variation in melt pool depth for 100 W power and combination of speed

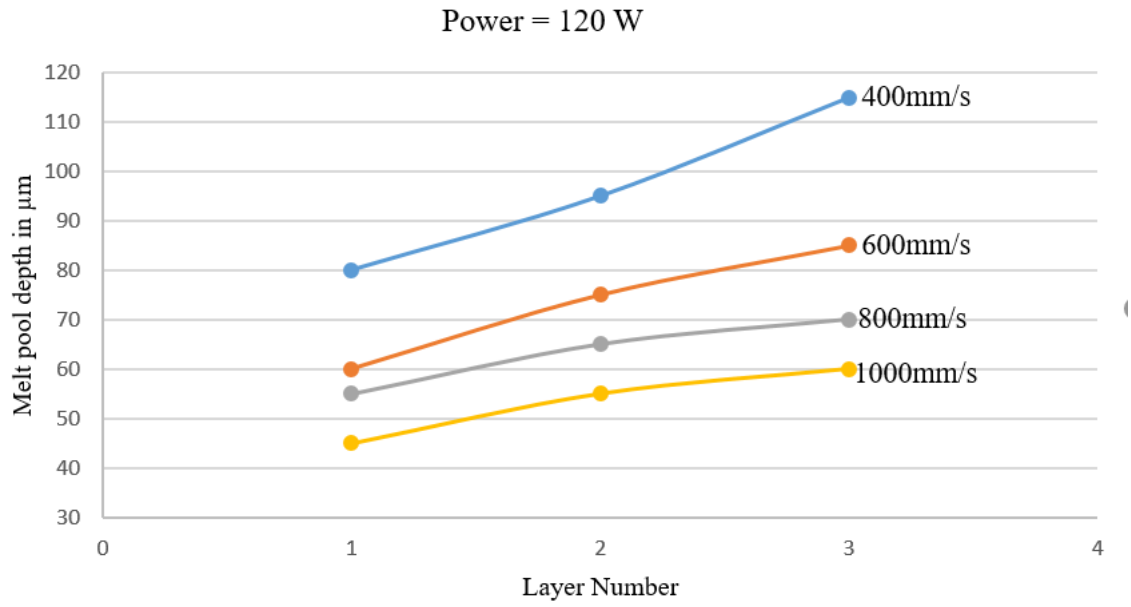

Figure 9.15: Variation in melt pool depth for 120 W power and combination of speed.

As can be seen from temperature behavior, the same trend is followed by melt pool behavior. At first layer, the melt pool depth is low. Because at first layer is totally surrounded by powder having very low conductivity. This results in lower heat dissipation into the surroundings and hence small melt pool. But as further layers are added, the temperature rises with subsequent layers. The reason for this as previously stated, the base

of melted and solidified pervious metal warm layer. So when the laser is incident it goes very deep into powder as well as previously solidified layer. Also reduction in speed results in deeper melt pool. Powder have more time to absorb the laser energy and laser has chance to reach deeper in case of lower scan speed.

10. CONCLUSION

The analysis is done on ANSYS using maraging steel material. The purpose of this study is to analyze the maximum temperature, temperature distribution and melt pool shape and dimensions. The graph of temperature and melt pool versus layers is plotted for different power and speed and following conclusions can be drawn.

1. The temperature rises with further addition of layers, but their difference in temperature decreases with addition of subsequent layers.
2. It has been observed that temperature increases with reduction in speed as high amount of energy impinges per unit volume.
3. The slope of temperature versus layers is high initially but reduces as further layers are added
4. The melt pool depth like temperature increases with increasing power and reducing speed, but rise is more with reducing speed as compare to increasing power.
5. Melt pool depth become deeper with subsequent layers because of the availability of warm and semi solid previous layer. Because of penetration depth more than layer thickness, the laser in addition to new layer also melts the lower layer.
6. Dimensions of melt pool increases with the reduction in speed, as powder have more time to absorb heat from laser.
7. The depth of melt pool increases with increasing power of laser. As more power results in more energy, which will melt high quantity of powder.

REFERENCE

[1] **EPMA** (2013). Introduction to Additive Manufacturing Technology. *Epma* 42.

[2] **Roland Berger** (2017). Additive Manufacturing in Aerospace and Defense. 37.

[3] **Frost & Sullivan's Global 360° Research Team** (2016). Global Additive Manufacturing Market 2023 - Forecast. *Frost & Sullivan* 20–25. Available from: http://www.statista.com/statistics/284863/additive-manufacturing-projected-global-market-size/

[4] **Url-1** <https://www.spilasers.com/whitepapers/practical-applications-and-uses-for additive-manufacturing/>.

[5] **Trevisan, F. *et al.*** (2017). On the selective laser melting (SLM) of the AlSi10Mg alloy: Process, microstructure, and mechanical properties. *Materials (Basel).* 10.

[6] **Roehling, T. T. *et al.*** (2017). Modulating laser intensity profile ellipticity for microstructural control during metal additive manufacturing. *Acta Mater.* 128, 197–206. Available from: http://dx.doi.org/10.1016/j.actamat.2017.02.025

[7] **Michaleris, P.** (2014). Modeling metal deposition in heat transfer analyses of additive manufacturing processes. *Finite Elem. Anal. Des.* 86, 51–60. Available from: http://dx.doi.org/10.1016/j.finel.2014.04.003

[8] **Salmi, A., Atzeni, E., Iuliano, L. & Galati, M**. (2017). Experimental Analysis of Residual Stresses on AlSi10Mg Parts Produced by Means of Selective Laser Melting (SLM). *Procedia CIRP* 62, 458–463. Available from: http://dx.doi.org/10.1016/j.procir.2016.06.030

[9] **Xing, J., Sun, W. & Rana, R. S.** (2013). 3D modeling and testing of transient temperature in selective laser sintering (SLS) process. *Optik (Stuttg).* 124, 301–304. Available from: http://dx.doi.org/10.1016/j.ijleo.2011.11.064

[10] **Franco, A., Lanzetta, M. & Romoli, L**. (2010). Experimental analysis of selective laser sintering of polyamide powders: An energy perspective. *J. Clean. Prod.* 18, 1722–1730. Available from: http://dx.doi.org/10.1016/j.jclepro.2010.07.018

[11] **Acharya, R., Sharon, J. A. & Staroselsky, A.** (2017). Acta Materialia Prediction of microstructure in laser powder bed fusion process. 124, 360–371.

[12] **Olakanmi,** (2008). E. O. Direct selective laser sintering of aluminium alloy powders. Available from: http://etheses.whiterose.ac.uk/1476/

[13] **German, R. M., Suri, P. & Park, S. J.** (2009). Review : Liquid phase sintering. *J. Mater. Sci.* 44, 1–39.

[14] **Dai, D. & Gu, D.** (2015). Tailoring surface quality through mass and momentum transfer modeling using a volume of fluid method in selective laser melting of TiC/AlSi10Mg powder. *Int. J. Mach. Tools Manuf.* 88, 95–107. Available from: http://dx.doi.org/10.1016/j.ijmachtools.2014.09.010

[15] **Mukherjee, T., Zuback, J. S., De, A. & DebRoy, T.** (2016). Printability of alloys for additive manufacturing. *Sci. Rep.* 6, 1–8.

[16] **Kempen, K. *et al.*** (2011). Process Optimization and micostructural analysis for Selective Laser Melting of AlSi10Mg. *Solid Free. Fabr.* 484–495.

[17] **Hiemenz,** (2007). J. Electron beam melting. *Adv. Mater. Process.* 165, 45–46.

[18] **Dutta, B., Singh, V., Natu, H., Choi, J. & Mazumder, J.** (2009). Direct Metal Deposition. *Adv. Mater. Process* 167, 33–36. Available from: http://mbraun.com/images/201/POM Group.pdf

[19] **Shellabear, M., Nyrhila, O.** (2013). Materials for direct metal laser-sintering. *Whitepaper* 1–10.

[20] **Uast, U. (2016).** Material Selection in Selective Laser Sintering Material Selection in Selective Laser Sintering Thesis Provided for Master of Engineering By : Tzung Lin. 0–9.

[21] **Bourell, D. *et al*.** (2017). Materials for additive manufacturing. *CIRP Ann. - Manuf. Technol.* 66, 659–681. Available from: http://dx.doi.org/10.1016/j.cirp.2017.05.009

[22] **Cyr, E. *et al.*** (2018). Fracture behaviour of additively manufactured MS1-H13 hybrid hard steels. *Mater. Lett.* 212, 174–177. Available from: https://doi.org/10.1016/j.matlet.2017.10.097

[23] **Ma, D., Stoica, A. D., Wang, Z. & Beese, A. M.** (2017). Crystallographic texture in an additively manufactured nickel-base superalloy. *Mater. Sci. Eng. A* 684, 47–53. Available from: http://dx.doi.org/10.1016/j.msea.2016.12.028

[24] **Das, S., Bourell, D. L. & Babu, S. S.** (2016). Metallic materials for 3D printing. *MRS Bull.* 41, 729–741.

[25] **Oyelola, O., Crawforth, P., M'Saoubi, R. & Clare, A. T.** (2016). Machining of Additively Manufactured Parts: Implications for Surface Integrity.

Procedia CIRP 45, 119–122.

[26] **Tang, M. & Pistorius, P. C.** (2017). Oxides, porosity and fatigue performance of AlSi10Mg parts produced by selective laser melting. *Int. J. Fatigue* 94, 192–201. Available from: http://dx.doi.org/10.1016/j.ijfatigue.2016.06.002

[27] **Asgari, H., Baxter, C., Hosseinkhani, K. & Mohammadi, M.** (2017). On microstructure and mechanical properties of additively manufactured AlSi10Mg_200C using recycled powder. *Mater. Sci. Eng. A* 707, 148–158. Available from: http://dx.doi.org/10.1016/j.msea.2017.09.041

[28] **Louvis, E., Fox, P. & Sutcliffe, C. J.** (2011). Selective laser melting of aluminium components. *J. Mater. Process. Technol.* 211, 275–284. Available from: http://dx.doi.org/10.1016/j.jmatprotec.2010.09.019

[29] **Casati, R., Lemke, J., Tuissi, A. & Vedani, M.** (2016). Aging Behaviour and Mechanical Performance of 18-Ni 300 Steel Processed by Selective Laser Melting. *Metals (Basel).* 6, 218. Available from: http://www.mdpi.com/2075-4701/6/9/218

[30] **EOS GmbH** (2011). Material Data Sheet - 18Ni300. 49, 6. Available from: http://ip-saaseoscms.s3.amazonaws.com/public/1af123af9a636e61/042696652ecc69142c8518dc772dc113/EOS_MaragingSteel_MS1_en.pdf

[31] **Yasa, E., Kempen, K. & Kruth, J**. (2010). Microstructure and mechanical properties of Maraging Steel 300 after selective laser melting. *Proc. 21st Int. Solid Free. Fabr. Symp.* 383–396. Available from: http://utwired.engr.utexas.edu/lff/symposium/proceedingsArchive/pubs/Manuscripts/2010/2010-32-Yasa.pdf

[32] **Wong, K. V. & Hernandez, A.** (2012). A Review of Additive Manufacturing. *ISRN Mech. Eng.* 2012, 1–10. Available from: http://www.hindawi.com/journals/isrn/2012/208760/

[33] **Yang, L. *et al.*** (2017). Additive Manufacturing of Metals: The Technology, Materials, Design and Production. 33–44. Available from: http://link.springer.com/10.1007/978-3-319-55128-9

[34] **Herzog, D., Seyda, V., Wycisk, E. & Emmelmann, C.** (2016). Additive manufacturing of metals. *Acta Mater.* 117, 371–392. Available from: http://dx.doi.org/10.1016/j.actamat.2016.07.019

[35] **Liu, J. & To, A. C.** (2017). Quantitative texture prediction of epitaxial columnar grains in additive manufacturing using selective laser melting. *Addit. Manuf.* 16, 58–64. Available from:

http://dx.doi.org/10.1016/j.addma.2017.05.005

[36] **Thijs, L., Kempen, K., Kruth, J. P. & Van Humbeeck, J.** (2013). Fine-structured aluminium products with controllable texture by selective laser melting of pre-alloyed AlSi10Mg powder. *Acta Mater.* 61, 1809–1819. Available from: http://dx.doi.org/10.1016/j.actamat.2012.11.052

[37] **Xu, W., Lui, E. W., Pateras, A., Qian, M. & Brandt, M.** (2017). In situ tailoring microstructure in additively manufactured Ti-6Al-4V for superior mechanical performance. *Acta Mater.* 125, 390–400.

[38] **Jägle, E. A. *et al.*** (2017). Comparison of maraging steel micro- and nanostructure produced conventionally and by laser additive manufacturing. *Materials (Basel).* 10.

[39] **Wallis, C., Buchmayr, B., Kitzmantel, M. & Brandstätter, E.** (2016). Additive manufacturing of Maraging steel on a copper substrate using selective laser melting. *Proc. 2nd Met. Addit. Manuf. Conf. (MAMC 2016)* 11.

[40] **EOS. Material Data Sheet (EOS)** (2014). - EOS MaragingSteel MS1. 49, 1–5. Availablefrom: https://cdn.eos.info/1deee2b550955632/b3615b80c80a/MS-MS1-M290_Material_data_sheet_10-17_en.pdf

[41] **Karl, M., Krafft, T. & Kelly, J.** (2014). Fracture of a Narrow-Diameter Roxolid Implant: Clinical and Fractographic Considerations. *Int. J. Oral Maxillofac. Implants* 29, 1193–1196. Available from: http://www.quintpub.com/journals/omi/abstract.php?article_id=14693#.VCWnWBavueU

[42] **Senthilkumaran, K., Pandey, P. M. & Rao, P. V. M.** (2009). Influence of building strategies on the accuracy of parts in selective laser sintering. *Mater. Des.* 30, 2946–2954. Available from: http://dx.doi.org/10.1016/j.matdes.2009.01.009

[43] **Kudzal, A. *et al.*** (2017). Effect of scan pattern on the microstructure and mechanical properties of Powder Bed Fusion additive manufactured 17-4 stainless steel. *Mater. Des.* 133, 205–215. Available from: http://dx.doi.org/10.1016/j.matdes.2017.07.047

[44] **Dietrich, S., Wunderer, M., Huissel, A. & Zaeh, M. F.** (2016). A New Approach for a Flexible Powder Production for Additive Manufacturing. *Procedia Manuf.* 6, 88–95. Available from: http://dx.doi.org/10.1016/j.promfg.2016.11.012

[45] **Tatiana Polivnikova.** (2015). Study and Modelling of the Melt Pool Dynamics during Selective Laser Sintering and Melting. 6826. Available from: https://infoscience.epfl.ch/record/213654/files/EPFL_TH6826.pdf

CURRICULUM VITAE

Name Surname **:** MOBIN MAJEED

Place and Date of Birth **:** INDIA, 20 SEPTEMBER 1993

E-Mail **:** mobeen414@gmail.com

EDUCATION

- **B.Tech.** **:** 2014, Aligarh Muslim University, Faculty of Engineering and Technology, department of Mechanical Engineering

PROFESSIONAL EXPERIENCE AND REWARDS:

- 2015-2016 Aligarh Muslim University Ergonomics laboratory.
- 2014 Excellence Performance Award, Islamic Development Bank Group.

UNDER REVIEW:

- **H.M. Khan, M. Majeed, M.H. Dirikolua, E. Koç, I. Rasheed** 2018, Analysis of melt pool behavior using finite element thermal analysis, *International Journal of light and electron optics*, ISSN: 0030-4026